Charles University in Prague
FACULTY OF SCIENCE

Department of Physical and Macromolecular Chemistry



Ellipsometry and fluorescence microscopy applied to model membranes

Adam Miszta

Supervisor:
Prof. Dr. Martin Hof, DSc.
Academy of Sciences of the Czech Republic

PhD thesis

Prague
2009

This PhD thesis describes my original work except where acknowledgement is made in the text. It is not substantially the same as any work that has been, or is being submitted to any other university for any degree, diploma or any other qualification.

Acknowledgements

The completion of my PhD thesis has been a long journey. I could not have succeeded without the invaluable support of a several people.

First, I want to express my deeply-felt thanks to my thesis advisor, Prof. Martin Hof, for his warm encouragement, genuine caring and thoughtful guidance. I really enjoyed working with him. In his lab I learned to design scientific experiments, to present data in a logical way, and to write a paper. He has always put faith in me during my PhD study.

I would also like to give a heartfelt, special thanks to Prof. Wim Th. Hermens for his scientific advice and knowledge and many insightful discussions and suggestions. His patience, flexibility and concern helped me to finish my PhD. He has been motivating, encouraging and enlightening.

My enormous debt of gratitude can hardly be repaid to my friend Radek Machaň, who assisted me with my work and helped with all my papers. I am also particularly thankful to my friends I have had the pleasure to work with: Piotr Jurkiewicz, Aleš Benda, Jan Sýkora and other people from J. Heyrovský Institute of Physical Chemistry in Prague (Czech Republic).

These acknowledgements would not be complete if I would not express my gratitude to my family. Without your love, motivations and support this thesis would not exist.

List of abbreviations:

AFM	- Atomic Force Microscopy
Crp-4	- Cryptdin-4
DOPC	- 1,2-dioleoyl--glycero-3-phosphocholine
DOPS	- 1,2-dioleoyl-*sn*-glycero-3-phospho-L-serine
DLPC	- 1,2-dilauroyl-sn-glycero-3-phosphocholine
FCS	- Fluorescence Correlation Spectroscopy
FLIM	- Fluorescence Lifetime Imaging Microscopy
GUVs	- Giant Unilamellar Vesicles
LSM	- Laser Scanning Microscopy
LUVs	- Large Unilamellar Vesicles
POPC	- 1-palmitoyl-2oleoyl-*sn*-glycero-3-phosphocholine
POPG	- 1-palmitoyl-2oleoyl-sn-glycero-3-phospho-(1'-sn-glycerol)
SPBs	- Supported Phospholipid Bilayers
STM	- Scanning Tunneling Microscopy
SUVs	- Small Unilamellar Vesicles
QCM-D	- Quartz Crystal Microbalance with Dissipation

Publications:

The PhD thesis is based on following publications:

***Paper I*:**

Miszta A., Van Deursen B., Hermens W.Th., Hof M.;

"*Absence of ethanol-induced interdigitation in supported phospholipid bilayers on silica surfaces*";

Langmuir, 2008, 24 (1), 19

Paper II:

Miszta A., Machan R., Benda A., Oulette A., Hermens W.Th., Hof M.;

"*Combination of Ellipsometry, Laser Scanning Microscopy and Z-scan Fluorescence Correlation Spectroscopy Elucidating Interaction of Cryptdin-4 with Supported Phospholipid Bilayers*";

Journal of Peptide Science, 2008, 14 (4), 503

Paper III:

Machan R., Miszta A, Hermens W.Th., Hof M.;

"Real-time monitoring of mellitin induced pore and tubule formation from supported lipid bilayers and its physiological relevance",

Chemistry and Physics of Lipids, submitted 2009

Paper IV:

Miszta A., Machan R., Hermens W.Th., Hof M.

"Peptide-Membrane Interactions Studied by Ellipsometry, Laser Scanning Microscopy, and Z-Scan Fluorescence Correlation Spectroscopy"

Published in "Membrane-active peptides: methods and results on structure and function" by IUL (International University Line, La Jolla, California,USA)

Conference Proceedings related to this PhD thesis:

"6th EBSA European Biophysics Congress", 14-18.7.2007, London, UK;

(Poster: "*Ellipsometry, LSM and Z-scan FCS: interaction of antimicrobial peptides with planar lipid bilayers*"; Abstract published in European Biophysics Journal, 2007, 36, Supplement 1; 81)

"The EBSA Young Biophysicists Satellite Meeting", 14.07.2007, London, UK;

(Poster: "*Optical methods elucidating action of antimicrobial peptides*")

"2nd Workshop on Biophysics of Membrane-Active Peptides", (1-4.4.2007), Lisbon, Portugal; ***First prize on The European Biophysical Societies' Association (EBSA) best poster contest***

(Poster: "*Combination of Ellipsometry, Laser Scanning Microscopy and Z-Scan FCS as a tool to Study Interaction of Antimicrobial peptides with supported phospholipids bilayers*")

"3rd Prague Seminar on Biophysics on Lipids", (29.11-2.12.2006) Praha, Czech Republic;

(Oral presentation: *„The effect of antibacterial peptides on membrane and ethanol-induced membrane interdigitation")*

"6th Annual Surface and Colloid Symposium:Lipid-Peptide Interactions and Biological Function"; (14-15.11.2006), Lund, Sweden;

(Poster: „*Interaction of antibacterial peptides with membrane: A combined Ellipsometry and Laser Scanning Microscopy*")

„Seminář '*Spektroskopická Elipsometrie'*"; (24-25.10.2006), Brno, Czech Republic;

(Oral presentation: "*Ellipsometry as a tool for study membrane formation and protein-membrane interactions on supported phospholipid bilayers*")

Further publications:

Paper V:

Miszta A., Gabrielska J., Przestalski S., Langner M.,;

"*The effect of phenyltin chlorides on osmodically induced erythrocyte haemolysis*"; Applied Organometallic Chemistry, Volume 19 (6), 736-741, 2005

Paper VI:

Gabrielska J., Przestalski S., Miszta A., Soczyńska-Kordala M., Langner M.;

"*The effect of cholesterol on the adsorption of phenyltin compounds onto phosphatidylcholine and sphingomyelin liposome membranes*";

Applied Organometallic Chemistry, Volume 18 (1), 9-14, 2004

Abstract

The following PhD thesis presents two optical experimental techniques: ellipsometry and confocal fluorescence microscopy, and focuses on their applications in investigation of supported phospholipid bilayers (SPBs). The thesis presents two studies. First one shows real-time effects of ethanol on supported phospholipid bilayers formed by adsorption of phospholipid vesicles on solid surface measured by ellipsometry. This study first time demonstrated that ethanol-induced membrane interdigitation, as demonstrated for free standing bilayers, does not occur in the supported membranes. The finding indicates that membranes formed on supports, even fused into confluent bilayers, may differ from free-standing bilayer in vesicles. The second study is based on the combination of ellipsometry with two fluorescence microscopy techniques (i.e.Laser Scanning Microscopy and Z-Scan Fluorescence Correlation Microscopy) to gain information on the interaction of antimicrobial peptides with SPBs. These techniques were used to compare the mechanisms of interaction of the two different antimicrobial peptides α-helical Magainin 2 and β-sheet Cryptdin-4. LSM shows appearance of inhomogeneities in spatial distribution of lipids in the bilayer after treatment with Crp-4. Ellipsometric measurements show that binding of Crp-4 does not significantly change the lipid structure of the bilayer (increase in adsorbed mass without a change in thickness of adsorbed layer). Furthermore, Crp-4 slows the lateral diffusion of lipids within the membrane as shown by Z-scan FCS. All changes of the bilayer induced by Crp-4 can be partially reversed by flushing the sample with excess of buffer. Magainin 2-bilayer interactions are significantly different, causing large loss of lipids and extensive damage to the bilayer. It seems likely that differences in peptide mode of action, readily distinguished using these combined experimental methods, are related to the distinctive β-sheet and α-helical structures of the respective peptides. Moreover, combinations of these optical techniques were used to monitor temporal evolution of effects of antimicrobial peptide melittin on supported phospholipid bilayers (SPBs). Under all conditions used in this study, two reproducible phenomena were observed. The first one is formation of pores in the SPB, which occupy approximately 40% of the bilayer. And second, simultaneous, effect is the formation of tubules of approximately 30 nm radius and length of the order of 10 μm. Flushing of the sample with excess of buffer removes most of the tubules, but it does not affect the pores.

Content

Introduction.....9

1. Ellipsometry applied to model membranes – ethanol induced interdigitation in supported phospholipid bilayers 10

1.1. Principles of null-ellipsometry.....10

1.2. Ellipsometry applied to model membranes.....16

1.3. Effect of ethanol on phospholipid bilayers (Paper I) 23

1.4. Influence of errors on ellipsometry results (Paper I) 25

2. Combination of ellipsometry, laser scanning microscopy and Z-scan FCS elucidating interactions of antimicrobial peptides with model membranes.....28

2.1. Principles of fluorescence microscopy – Laser Scanning Microscopy and Z-Scan Fluorescence Correlation Spectroscopy (FCS).....29

2.2. Antimicrobial peptides.....39

2.3. Interactions of antimicrobial peptides with model membrane – combination of ellipsometry and fluorescence microscopy (Paper II and Paper III).....40

References: 55

Introduction

Ellipsometry and fluorescence microscopy are both techniques that have been known for years. Ellipsometry was mainly used to investigate and to characterize thin films on solid surfaces. *In-situ* ellipsometry, even though is a powerful tool, which gives the information about surface mass, thickness and refractive index (density) of the adsorbed layer is a complicated technique. The main problems of this technique are complicated calculations of the ellipsometric parameters and interpretation of the results. The calculations are very important to obtain correct final results because small variations in such parameters as refractive index of buffer or refractive index of solid support can give incorrect results. The strong point of ellipsometry is *in-situ* real-time monitoring of the events in a thin film between two media with sub-nanometer precision.

Fluorescence microscopy is a well-known technique used to visualize the structures and diffusion properties of the molecules. The main drawbacks of this method are poor resolution (~240 nm) and the necessity of using fluorescence chromophores, which can influence the measurement system.

In view of recent doubts on the validity of using supported phodpholipid bilayers (SPBs) as biological model membranes we first used ellipsometry for *in-situ* measurement of the real-time effects of ethanol on supported phospholipid bilayers. Secondly, we combined ellipsometry with two complementary optical techniques, laser-scanning microscopy (LSM) and Z-scan fluorescence correlation spectroscopy (FCS) to acquire comprehensive information on the mechanisms of the interactions of antimicrobial peptides with supported phospholipid bilayers (SPBs) .

The thesis is divided into two main chapters. First chapter deals with an introduction to ellipsometry and the production of supported phospholipid bilayers. It gives an overview of main aspects and explains the advantages of ellipsometry as a method to study SPB formation, that is, the transition of adsorbed phospholipid vesicles into fused bilayers at constant surface mass. The second part of this chapter presents the study of effect of ethanol on phospholipid bilayers. The main problems and errors that may occur in ellipsometric measurements are also discussed.

Second chapter deals with the interaction of SPBs with antimicrobial peptides. The first part presents an overview of LSM and Z-scan FCS as used to study the diffusion properties of supported phospholipid bilayers. The basic principles of each of the technique

are explained and their possibilities and limitations are discussed. The second part gives an introduction to antimicrobial peptides. The last part presents the combination of those fluorescence techniques with ellipsometry to gain information on the interaction mechanisms of antimicrobial peptides with SPBs.

1. Ellipsometry applied to model membranes – ethanol induced interdigitation in supported phospholipid bilayers

The first ellipsometric studies were performed by Tronsted in 1932[1]. He used the length of fatty acid chains to test the validity of the Drude equations for thin transparent films on metal surfaces. Among other pioneering works are studies of the kinetics of protein adsorption by Vroman [2] and the immunological research of Rothen[3-5]. However, even though ellipsometry appears to find applications in life science over many years, it has only been used by a small numbers of research groups, mainly in physical chemistry.

The first chapter brings an overview of ellipsometry technique. This technique will be introduced in details as a powerful technique for in situ real-time monitoring of phospholipid membranes.

1.1. Principles of null-ellipsometry

Ellipsometry is an accurate and non-destructive optical technique used to observe and characterize the materials and events in thin films on solid surfaces. It is based on the measurement of light before and after reflection from a surface. The interaction of light with the sample causes a change in the polarization state of light. Such changes can be then analyzed and used to characterize the thickness and refractive index of thin films on surfaces with sub-nanometer precision. A major advantage of ellipsometry is its ability to make quantitative *in situ* measurements of processes at solid/liquid interface. The setup, however, for studies of organic layers (e.g., phospholipids, peptides, or polymers) in solution is more difficult and complicated compared with the standard ellipsometry setup used in semiconductor science.

1.1.1. Experimental setup

The most popular type of ellipsometry is null ellipsometry shown in figures 1[6, 7]. The configuration of null ellipsometry consists of a light source, linear polarizer, compensator, sample, analyzer and detector. The initial polarization state of light incident on the sample is determined by the light source, polarizer and compensator, and the analyzer and detector are used to detect the change in polarization. This method is based on finding a set of angles for polarizer, compensator, and analyzer at which the light in the detector is extinguished. The principle of null ellipsometry is rather simple. First circular monochromatic light (λ=632 nm) emitted by a light source passes through a polarizing prism (the polarizer). As a result plane-polarized light is emitted. Next, the light by passing through the compensator, changes to elliptically polarized light. The resulting elliptically polarized light is reflected from the surface and passes through a second polarizing prism (the analyzer). The positions of the polarizer P and the analyzer A are rotated such that the final light intensity, as detected by photodiode, becomes zero (figure 2).

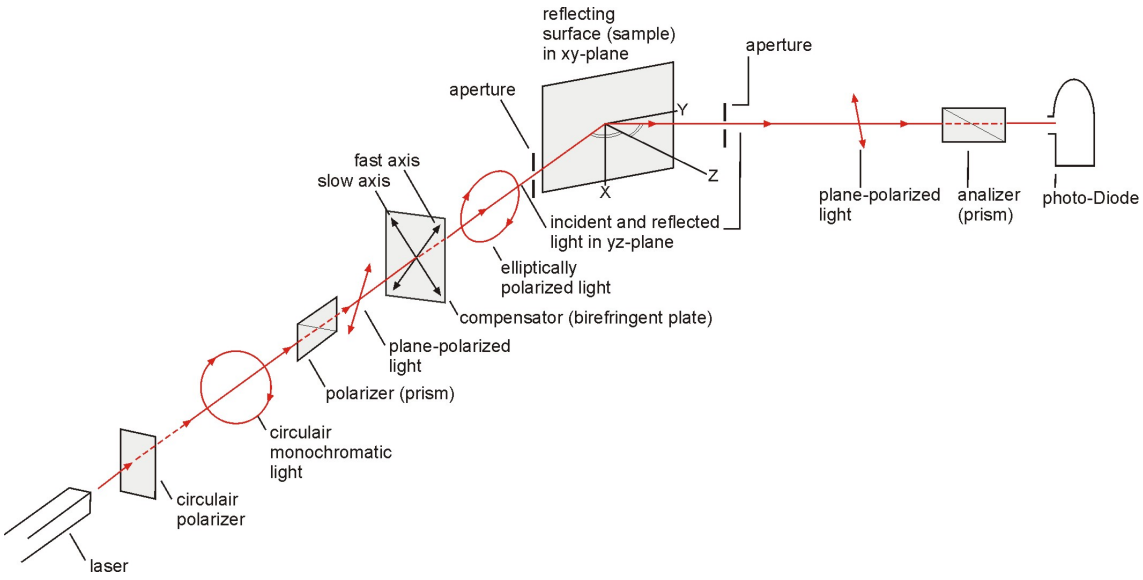


Figure 1. Scheme of the ellipsometer.

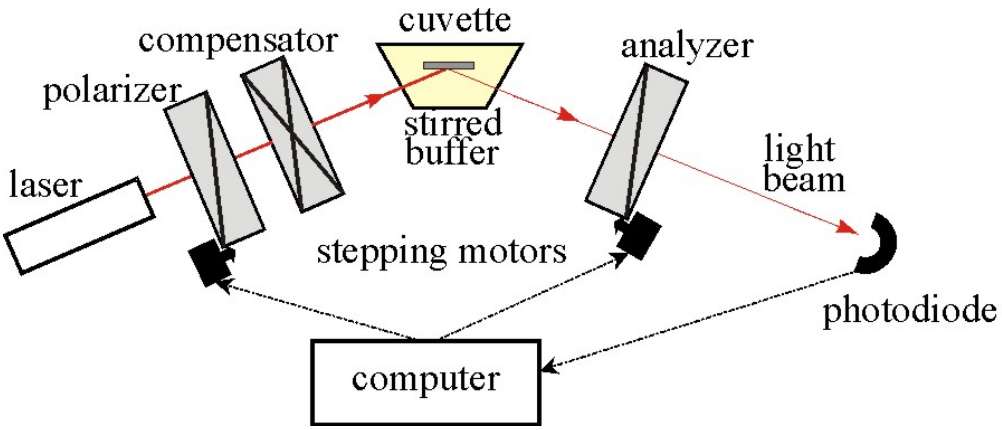


Figure 2. Scheme of the automated null-ellipsometer with stepping motors and computer

The major advantage of null ellipsometry in life sciences is that it allows real-time *in-situ* measurements. Such *in-situ* experiments can be performed on slides immersed in a (buffer) solution. It is hard to design a universal cell for different types of experiments but some main aspects of cell design can be considered. The most obvious aspects are cell volume, stirring, exchange of liquid, angle of incidence, window properties and sample mounting. An example of an open cell design is shown in Figure 3 [8]. The first and very important aspect that has to be discussed is cell volume. Large volumes may require too large quantities of adsorbing substances and small volumes may cause depletion of such substances in the buffer.

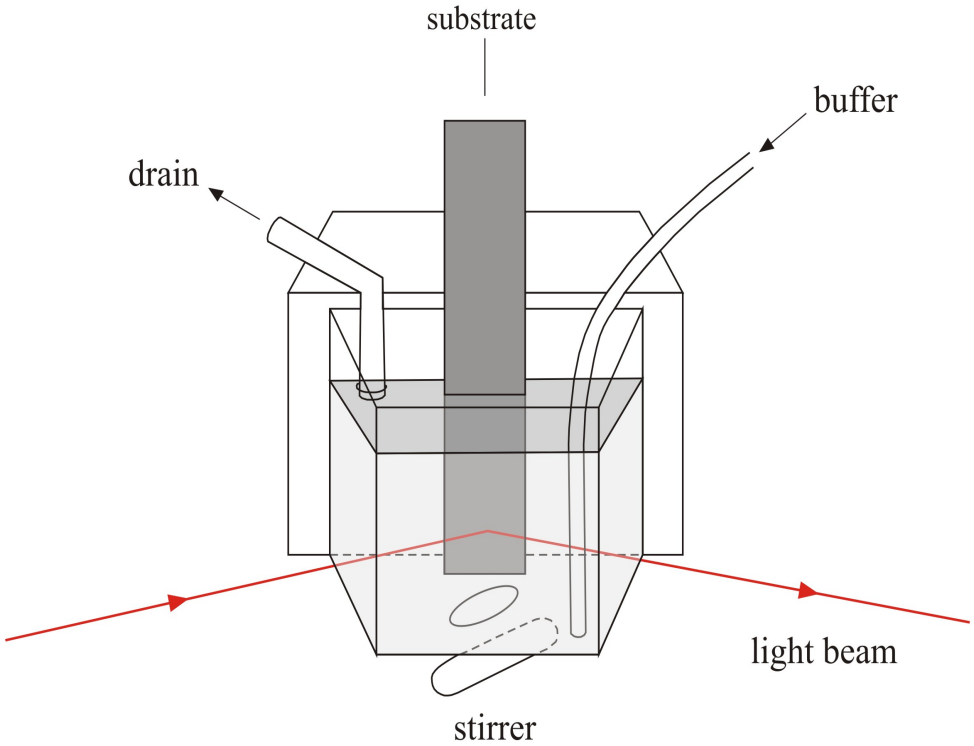


Figure 3. Ellipsometer cell for in situ studies at solid/liquid interface.

Second important aspect is stirring because without effective stirring the adsorbing substances that can only reach the surface by diffusion and adsorption, becomes slow [9]. This problem can be solved by using a Teflon stirrer or in the smaller cell, by use of a flow cell [10]. It was shown that stirring is important in the adsorption of many proteins or phospholipids. Another important aspect is sample mounting. In the model showed in figure 3 the sample is immersed into the liquid from above. The drawback of this design is that long (several cm) substrates are needed. The advantage however is that sample and cell with liquid can be aligned separately. The windows in the cell are very important because they may introduce systematic error in ellipsometric data due to optical imperfections. The walls of the cuvette, mainly made from glass or quartz, have to be preferably designed perpendicular to the light beam to minimalize optical refraction effects [8].

1.1.2. Determination of ellipsometric parameters

Ellipsometry is an indirect technique i.e. in general the measured angles of the polarizer and the analyzer cannot be converted directly into the optical constants of the sample. Thus, a model analysis must be performed. The principle of ellipsometry is to adjust the polarizer P and the analyzer A in such a position that the intensity of the passing light is minimal, ideally null. Direct conversion of measured values of P and A into finally results is only possible for isotropic, homogenous and rather thick samples [7]. In all other cases a layer model must be established, which considers the optical constants (refractive index and thickness) of all individual layers of the sample.

The basic equation of ellipsometry is:

$$\tan \Psi e^{i\Delta} = \frac{R_p}{R_s} \tag{1.1}$$

where the two angles Ψ and Δ can be directly obtained from P and A and R_p and R_s are the total reflection coefficients for light polarized in the direction parallel and normal to the plane of incidence.

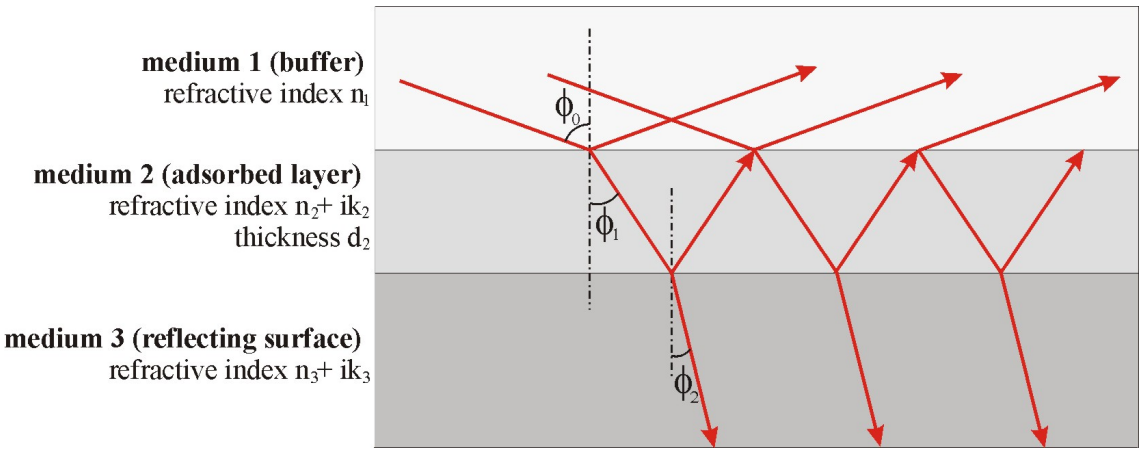


Figure 4. Scheme of three-layer model used for ellipsometry calculation.

The thickness and refractive index of thin layer adsorbed on the solid surface can be calculated using an optical three-layer system (Figure 4). In this model the first medium is the solution (buffer or water) with refractive index n_1 and angle of incidence ϕ_1. The second medium is the thin film (mixture of buffer, peptides and phospholipids) adsorbed on the reflecting surface with refractive index n_2, thickness d_2, and angle of incidence ϕ_2. The third medium is the reflecting substrate (glass, mica, or silicon slide) with refractive index n_3 and angle of incidence ϕ_3. Note that the refractive indexes may contain complex parts k, with n determining the refraction and the absorption of light.

The complex values of R_p and R_s described in eq 1.1 for the three-layer system are calculated from the relations

$$R_p = \frac{(r_{p12} + r_{p23}e^{(D)})}{(1 + r_{p12}r_{p23}e^{(D)})} \tag{1.2}$$

and

$$R_s = \frac{(r_{s12} + r_{s23}e^{(D)})}{(1 + r_{s12}r_{s23}e^{(D)})} \tag{1.3}$$

where

$$D = \frac{-4\pi i d_2 n_2 \cos(\phi_2)}{\lambda} \quad , \; i=\sqrt{-1} \tag{1.4}$$

In these expressions, $\cos(\phi_2)$ is calculated from Snell's law:

$$\cos(\phi_2) = \left[1 - \left(\frac{n_1 \sin(\phi_1)}{n_2}\right)^2\right]^{\frac{1}{2}} \tag{1.5}$$

and the Fresnel coefficients r_{p12} and r_{s12} at the 1,2-interface are given by

$$r_{p12} = \frac{(n_2 \cos(\phi_1) - n_1 \cos(\phi_2))}{(n_2 \cos(\phi_1) + n_1 \cos(\phi_2))} \tag{1.6}$$

and

$$r_{s12} = \frac{(n_1 \cos(\phi_1) - n_2 \cos(\phi_2))}{(n_1 \cos(\phi_1) + n_2 \cos(\phi_2))} \tag{1.7}$$

with similar relations for r_{p23} and r_{s23}. The value of n_3 is calculated from the relation

$$n_3 = n_1 \tan(\phi_1)\left[1 - \frac{4\rho \sin^2(\phi_1)}{(\rho+1)^2}\right]^{\frac{1}{2}} \tag{1.8}$$

where

$$\rho = \tan(\Psi)e^{(i\Delta)} \tag{1.9}$$

and it is directly determined from ellipsometry measurements on the base substrate. The main problem in the calculations is that the two parameters d_2 and n_2 cannot be directly expressed in the angles Δ and Ψ and the optical constants of the system [7]. Thus to calculate these values a fitting procedure has to be used. Equation 1.1 for R_p and R_s can be written as a quadratic expression of the form

$$C1(e^{(D)})^2 + C2e^{(D)} + C3 = 0 \tag{1.10}$$

where $C1$, $C2$, and $C3$ are complex functions of the refractive indices, angles of incidence, Δ and Ψ. For the phospholipids and peptides as used in this study, the imaginary part of the refractive index n_2 is zero because adsorbed layers of organic compounds are generally nonabsorbing in the VIS (Visible Spectroscopy) region. For a real arbitrary value of n_2, two complex values of d_2 are obtained. To determine the correct values of refractive index n_2 and thickness d_2, adjustment of n_2 minimizes the imaginary complex part of d_2 (because the thickness must be real).

Alternatively, a more direct method can be used by minimizing the expression $(\Delta_{calculated} - \Delta_{measured})^2 + (\Psi calculated - \Psi_{measured})^2$ by adjustment of the value of d_2 and n_2 (2-parameter fitting). If we know the chemical composition of the adsorbed layer, the surface mass of the thin film can be calculated from the Lorentz-Lorentz equation [11]. This method requires knowledge of thickness, refractive index, molecular weight M, molecular refractivity A and specific volume ν of the molecules adsorbed on the surface. The equation for calculation the surface mass from the Lorentz-Lorentz relation is

$$\Gamma = 0.1 d_2 \left(\frac{L(n_2) - L(n_1)}{\frac{A}{M} - \nu L(n_1)} \right) \tag{8.11}$$

where n_1 is the refractive index of liquid (e.g., for water n=1.33211), d_2 and n_2 are thickness and refractive index of the layer adsorbed on the surface, respectively. The factor 0.1 in equation (8.11) enters because the thickness d_2 is expressed in nanometers and the surface mass Γ is obtained in micrograms per square centimetre. L is defined as $L(n_i) \equiv (n_i^2 - 1) / (n_i^2 + 2)$. The A/M ratio and the ν value depend on the compounds present in the adsorbed layer (e.g., for albumin A/M = 0.234, ν = 0.729; for prothrombin A/M = 0.236, ν = 0.700; and for DOPC/DOPS (4:1) lipids A/M = 0.274, ν = 0.890). More details about molar refractivity and weight can be found in Cuypers et al. [11].

Two strong points of ellipsometry are that the reflecting solid surfaces (glass, mica, silicon) used for experiments are inexpensive and the surface mass determined by ellipsometry is well defined with high precision, especially on silicon. Another advantage of ellipsometry compared to other scanning techniques like AFM or STM (scanning tunnelling microscopy) is a possibility to simultaneous measurement of fast changes of condensation of adsorbed lipids into bilayer in relatively large surface area.

This technique has also a few weak points. The lateral resolution of ellipsometry is poor because it uses an unfocused measurement light beam. Systematic errors are caused by surface roughness, which for some surfaces can be in the order of the bilayer thickness and by imperfections of the optical components, such as nonideal polarizers or differences in light transmission along the two axes of the compensator, that causes experimental error. Furthermore, the ellipsometry does not give any chemical information about the sample, so it is difficult to determine what substance we actually measure. Moreover, for membrane-peptide interactions there is no identification of different mass components.

1.2. Ellipsometry applied to model membranes

Biological membranes play a crucial role in cell biology. Their major functions are separating and maintaining the communication between inside and outside cellular worlds

and participating in various extra- or intracellular processes [12]. Cellular membranes are dynamic structures composed of a diverse set of phospholipid molecules held together by hydrophobic interactions and proteins embedded within the phospholipid layer. Phospholipid molecules, composed of a hydrophilic head group and two hydrophobic acyl chains, have the unique ability to self-assembly into two-layered sheets so called the phospholipid bilayers. These phospholipid bilayers consist of two adjacent layers, with the hydrophilic headgroup exposed to water and hydrophobic chains hidded in the bilayer interior.

1.2.1. Supported phospholipid bilayers

Many models have been proposed to mimic biological membranes, including black lipid membranes, unilamellar vesicles (small, large and giant), lipid monolayers at air-water interface and supported phospholipid bilayers. All models resemble cell membranes in some key respects. Very popular model membrane in last years is the supported phospholipid bilayer (SPBs) (Figure 5) [13, 14].

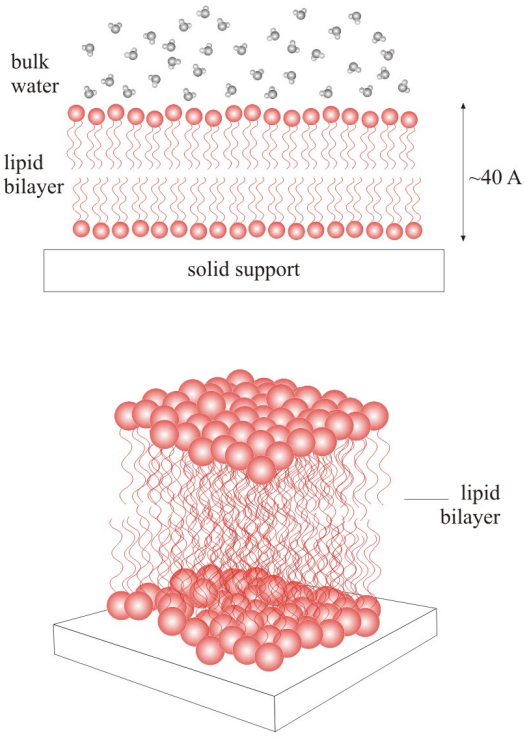


Figure 5. Schematic diagram of a supported phospholipid bilayer (SPB).

A multitude of different methods have been proposed to create SPBs. The most common are adsorption, fusion, and rupture of lipid vesicles or micelles on solid hydrophilic surfaces as developed by Tamm and McConnel [15-23] and the earlier techniques as Langmuir-Blodgett or Langmuir-Schafer deposition, based on transfer of two monolayers from the air-water interface to a hydrophilic support [24, 25] . However all methods have some drawbacks and advantages. For example, transfer of amphiphilic molecules from air-water interface to solid substrates has the big advantage of being able to form asymmetric bilayers [26], but it is very difficult with this technique to incorporate transmembrane proteins into the lipid bilayer. The main problem is that some parts of the proteins within the lipid monolayer are exposed to air and can become irreversibly denaturated [27]. This problem is very easily solved for lipid vesicles. The incorporation of transmembrane proteins into vesicles involves a gentler process such as detergent removal via dialysis [28, 29].

SPBs have opened the new door for surface-sensitive analytical techniques such as surface plasmon resonance (SPR) [17], total internal reflection fluorescence (TIRF) [30], atomic force microscopy (AFM) [31-33], quartz crystal microbalance with dissipation monitoring (QCM-D) [17, 34], or ellipsometry [25]. It was shown that supported phospholipid bilayers have a big potential for biomedical research and applications. The fluid two-dimensional structure of SPB allows of lipid molecules free rotation and lateral diffusion within the bilayer. This property makes them a suitable model to investigate binding of peptides [11, 35-37].

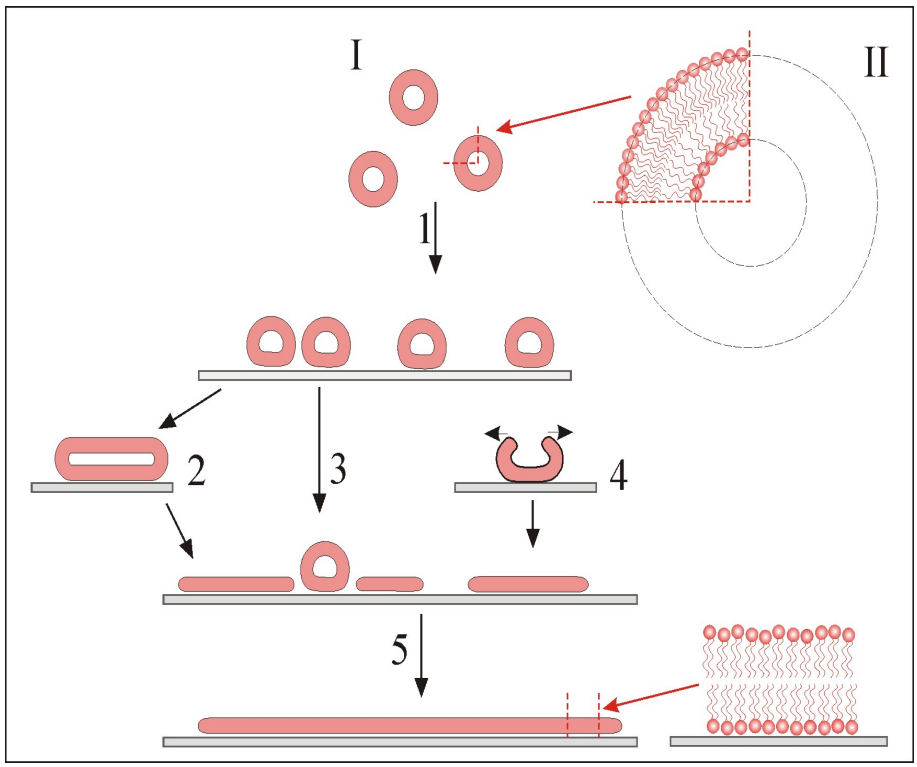


Figure 6. I. Scheme of possible mechanisms in the formation of SLBs by deposition of lipid vesicles (from Richter, Biophysical Journal 2003). 1) Adsorption and deformation of vesicles. 2) Interaction between the vesicles and fusion to supported membranes. 3) Interaction of vesicles with membrane patches. 4) Individual rapture of lipid vesicles to SPBs. II. Cross-section of lipid vesicles.

Several factors, such as surface charge, surface roughness, surface cleanliness, vesicle composition and size, solution pH, temperature, osmotic pressure and ionic strength, have been identified to influence the adsorption of lipid vesicles on solid surfaces and the formation of bilayers [14, 38, 39]. It is well established that phopholipid bilayers on solid surfaces are held in place by a combination of van der Waals, electrostatic, hydration and steric forces [40]. The exact mechanism of the bilayer formation from vesicles fusion is not fully understood, however some models have been proposed [33, 34] (figure 6).

1.2.2. Ellipsometry applied to model membranes

The first ellipsometric study of lipid bilayers was performed in 1980, by Cuypers et al. [41], who used ellipsometry to study the temperature-dependent transitions in several phospholipids layers. Since that pioneer work the ellipsometry was mainly used to study the peripheral or integral binding of peptides [11, 42]. Detailed studies of the membrane formation process were done by Benes et al, 2004 [43]. It was shown that ellipsometry is a powerful technique to monitor self-assembling phospholipid membranes on solid surface.

Moreover, the work of Benes provides information on surface mass, thickness and refractive index (density) of the phospholipid bilayer, and thereby not only on SPB adsorption but also on the transition (kinetics) of supported phospholipid vesicles into confluent bilayers. An example of bilayer formation on a silica surface is shown in figure 7. This plot shows two phases. The first phase is adsorption of phospholipids vesicles on solid surface (phase A) and the second phase the formation of bilayers on silica surface (phase B). From the fact that vesicle fusion occurs only when about half of total surface mass is reached and does not occur when adsorption is interrupted before that surface mass is reached (Figures 8A and 8B.) it is concluded that fusion will only occur when the vesicles come into contact with each other.

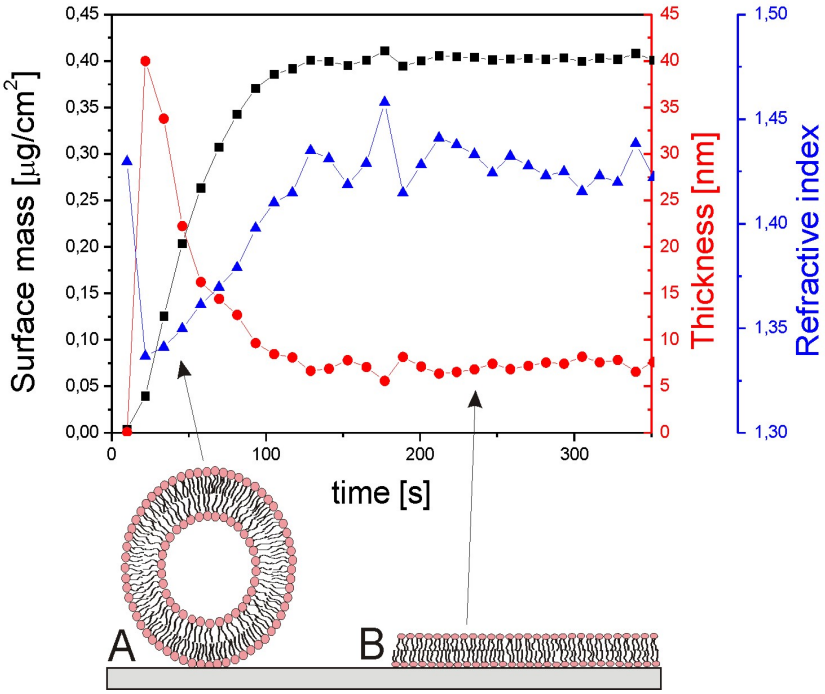


Figure 7. Formation of SPBs. Time evaluation of surface mass (-■-), thickness (-●-) and refractive index (-▲-) after addition of 20mM of DOPC/DOPS (80/20%) lipid vesicles to a silica surface in the present of 2mM calcium. "A" indicates adsorption of lipid vesicles on solid support; "B" indicates formation of bilayers. Data obtained by author.

Adsorbed lipid vesicles on silicon oxide have an initial average thickness of 40 nm and refractive index of about 1.340 (close to refractive index of pure buffer 1.335). These vesicles may immediately start to rupture and transform into a bilayer disk or first fuse and interact with neighbouring vesicles and then rupture into membrane patches (figure 6). Finally a condensed, thinner and denser layer is observed with a surface mass of about 0.40 mg/cm^2, a thickness of about 7 nm and refractive index of about 1.40. These results

however differ for different solid surface, membrane and buffer composition (table 1) [43]. For example, it was shown that bilayers created on glass surfaces are thicker and denser compared to membranes formed on mica or silicon. The SPB can be formed by fusion of lipid vesicles on a hydrophilic surface such as silica, glass or mica but not on titanium oxide or gold. On these special supports the lipid vesicles layer is formed but the vesicles do not rupture to form a bilayer. To confirm the above-mentioned conclusions about the formation of bilayers, ellipsometry was combined with other surface technique like AFM and QCM-D [34, 37, 44].

Table 1. Formation of membranes from SUV's in Hepes buffer.
The concentration of phospholipids was 100 μM. (Data from Benes 2004)

Silicon oxide			***Mica***			***Glass***		
Surface mass ($\mu g/cm^2$)	Thickness (nm)	Refractive Index	Surface mass ($\mu g/cm^2$)	Thickness (nm)	Refractive Index	Surface mass ($\mu g/cm^2$)	Thickness (nm)	Refractive Index
Membrane composition: DOPC/DOPS (80/20%) + EDTA								
0.36	11	1.39	~0.36	~10	~1.42	0.45	13	1.39
Membrane composition: DOPC/DOPS (80/20%) + Ca^{2+}								
0.38	9.9	1.40	0.66	10	1.45	0.54	13	1.42
Membrane composition: DOPC + Ca^{2+}								
> 0.41	>41	<1.35	0.55	20	1.38	0.49	>17	<1.38
Membrane composition: DOPC + EDTA								
> 0.51	> 80	< 1.34	~ 0.9	~ 40	~ 1.38	0.41	> 24	>1.36

As shown in table 1, thick layers will have low refraction indexes and in the absence of calcium no vesicles fusion occurs on mica. The fact that also on silica layers remain thicker than the 6-7 nm of a double layer [43] indicates that some vesicles adhere to the membranes or to the surface in between confluent membrane, although some estimation of thickness could also be due to systematic error in the ellipsometer readings.

Figure 8A shows the effect of calcium, which is required for bilayer formation at such low lipid concentration. Figure 8B shows the effect of critical vesicular coverage, which is needed to trigger the transformation of liposomes into a continuous bilayer. During vesicle adsorption the cuvette was flushed with buffer after adsorption of 200

ng/cm^2 of lipids (about half of a complete bilayer). The adsorbed vesicles remain stable and do not fuse into a bilayer. In the same experiment the cuvette with adsorbed vesicles was flushed with low anionic strength buffer to induce vesicle fusion by an osmotic shock. One observes a significant swelling of vesicles by intake of water but no fusion of vesicles.

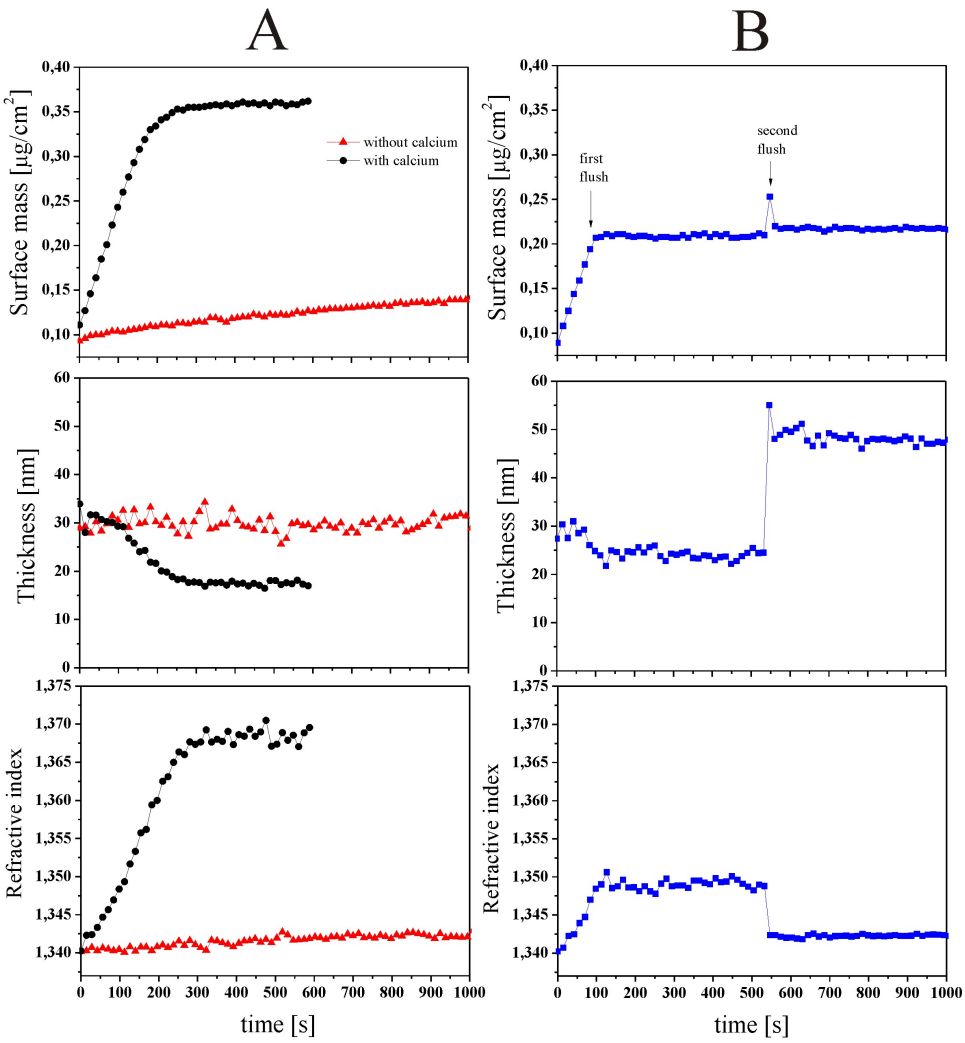


Figure 8. Membrane formation on silicon oxide for low phospholipid concentration. Panel A shows adsorption of 5µM of sonicated DOPS/DOPC (4:1) vesicles in 50 mM Tris-NaCl buffer (pH 7.5) (100 mM NaCl) with (-▲-) and without 3 mM of $CaCl_2$ (-●-). These results show that for a low lipid concentration the calcium apparently is required for vesicle fusion. Panel B shows adsorption of 5µM of sonicated DOPS/DOPC (4:1) vesicles in 50 mM Tris-100mM NaCl buffer (pH 7.5) (-■-) with 3 mM of $CaCl_2$. In the plot "First flush" indicates that the vesicles were removed by flushing after adsorption of 200 ng/cm^2 of lipid (about half of a complete bilayer). "Second flush" indicates that the vesicles were flushed with 5 mM Tris-NaCl buffer (pH 7.5) (10 mM NaCl) to induce vesicle fusion by an osmotic shock. Data obtained by author.

1.3. Effect of ethanol on phospholipid bilayers *(Paper I)*

The physiological effects of alcohols have been related to their effects on phospholipid packing in biological membranes. More specifically it has been shown that alcohols induce overlap of the alcyl chains from opposing monolayers (interdigitation), causing membrane thinning and higher packing density, not only because of chain overlap but also due to increasing tilt angles [45, 46]. In such interdigitated membranes, alcohol molecules are located in the chain region, near the phospholipid head groups [47].

Membranes deposited on solid supports by adsorption of unilamellar phospholipid vesicles have been used in many areas of biomedical research such as cell recognition in immunology [16], membrane-mediated thrombin production [48], membrane effects of anesthetics [49], and antimicrobial peptides [50]. In most of these studies cellular membrane composition was mimicked by excess phosphatidylcholine (PC), with fractions of negatively charged phospholipids like phosphatidylserine (PS) or phosphatidylglycerol (PG). Recently, accumulating evidence has cast some doubts on the validity of using supported phospholipid bilayers as cell membrane models and, because of its sensitivity to membrane properties, interdigitation seems a well suited parameter to detect possible effects of the supporting solid surface on membrane properties.

In the present section the effects of ethanol on DOPC/DOPS membranes on silica surfaces is investigated. This model membrane has been shown to consist of confluent bilayers [34, 43]. Results were compared with membranes prepared from pure DOPC and DLPC. Membranes were studied by ellipsometry, a technique that is well suited to monitor in situ changes of membranes thickness and packing [43].

Figure 9, shows that the effects of ethanol are fully reversible and the initial values for surface mass, thickness and refractive index are recovered when the ethanol is flushed away and replaced by pure water. For DOPC/DOPS (80/20 mol%) membranes, vesicle fusion into bilayers was confirmed by a final surface mass of about 0.39 $\mu g/cm^2$ and a low thickness of about 6 nm[43]. For DOPC and DLPC an average thickness of about 18 nm suggests adsorbed vesicles or mixed bilayer/vesicle membranes. DOPC/DOPS bilayers did not show reduced thickness after addition of ethanol, indicating that no interdigitation occurred. For DOPC and DLPC membrane swelling was observed, instead of the membrane thinning occurring during interdigiation. Because surface mass resumes its initial value after removal of ethanol, the latter would imply that 75 % of membrane mass

would consist of ethanol, which is obviously impossible without dissolving the membrane. It is concluded that ethanol-induced interdigitation is absent in these supported bilayers.

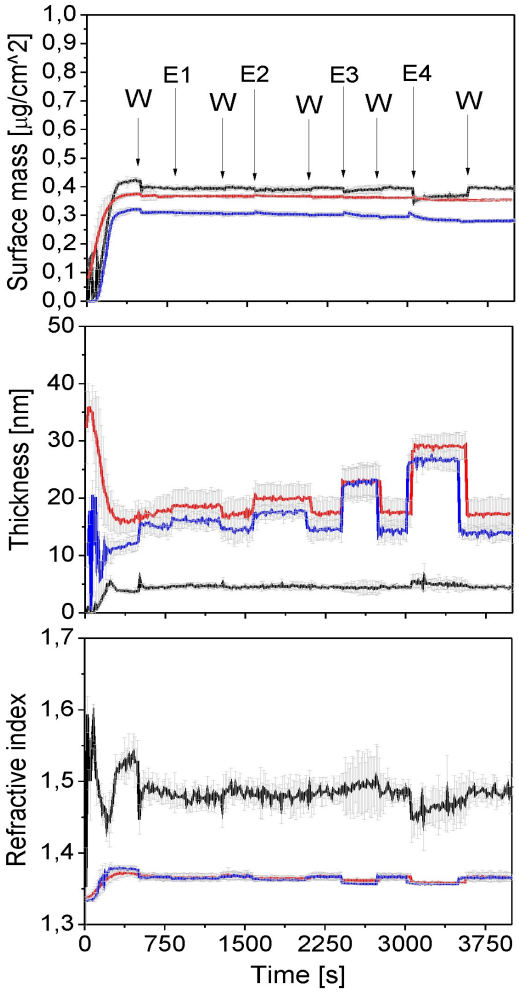


Figure 9. Surface mass, thickness and refractive indexand of DOPC/DOPS (black), DOPC (red) and DLPC (blue) membranes after addition of ethanol. “E1”, “E2”, “E3” and “E4“ in the graph indicate addition of ethanol, 1.6, 3.2, 6.2, and 11.7 vol%, respectively. “W” in the graph indicate flushing with pure water. Data from Miszta 2008.

These results indicate that membranes formed on supports - even when fused into confluent bilayers - may differ from free-standing bilayers in vesicles. For instance, PC/PS bilayers formed on mica showed accumulation of PS in the inner leaflet [19], and lateral diffusion in PC bilayers on silica was 2 times slower than in giant vesicles [51], possibly caused by lipids sticking to the support [52].

Using a variety of techniques like calorimetry, X-ray scattering, spectroscopy and fluorescence, ethanol-induced membrane interdigitation has been shown to be a general phenomenon in free-standing phospholipid bilayers. This study for the first time shows

real-time effects of ethanol on supported bilayers and demonstrates that in such preparations interdigitation seems to be absent. Apparently, the interactions between the lipids and the support surface interfere with this phenomenon.

This result seems at variance with a few AFM studies that claimed interdigitation in supported membranes [53, 54]. However, because of the difficulties in studying phospholipids in their fluid state with AFM, these studies used di-palmitoyl-PC (DPPC), which has a high transition temperature (41°C). As a result, these authors were unable to measure real-time transitions but heated their preparations to about 60°C, with and without ethanol, measuring the membrane changes after cooling down again. This could cause freezing of transitions that would have occurred in fluid-state phospholipids as found predominantly in biological membranes and used in the present study.

1.4. Influence of errors on ellipsometry results *(Paper I)*

Even though ellipsometry is a relatively simple optical technique, the results are sensitive to many different factors (e.g. refractive index of buffer or refractive index of solid support), which may introduce error. In this section the sources and influence of such error are discussed.

A very important aspect is that obtained values of d_2 and n_2 depend on each other. Overestimation of d_2 will cause underestimation of n_2 and vice versa. Because the surface mass Γ depends on the product of d_2 and n_2, the scatter for Γ is smaller than for d_2 and n_2. Use of fixed refractive index values n_2 of the adsorbed phospholipid layers, as often done in the literature, makes it impossible to detect membrane transitions at constant surface mass, such as fusion of adsorbed vesicles into bilayers. Without the correct values of n_2, a decrease in thickness d_2 will not follow from the calculations [43].

Apart from inherent experimental scatter, systematic error may also occur, for instance due to a non-ideal compensator or inadequate optical alignment of the instrument. Due to these factors, the *changes* in surface mass, thickness and refractive indices of adsorbed layers can be measured more accurately than the absolute values. Taking account of these circumstances, the error of surface mass as determined by ellipsometry is approximately 1 to 5 ng/cm^2 (this is ~1% of the bilayer); of thickness, 0.1 to 1 nm (depending on the reflecting surface); and of refractive index, 0.001 to 0.01.

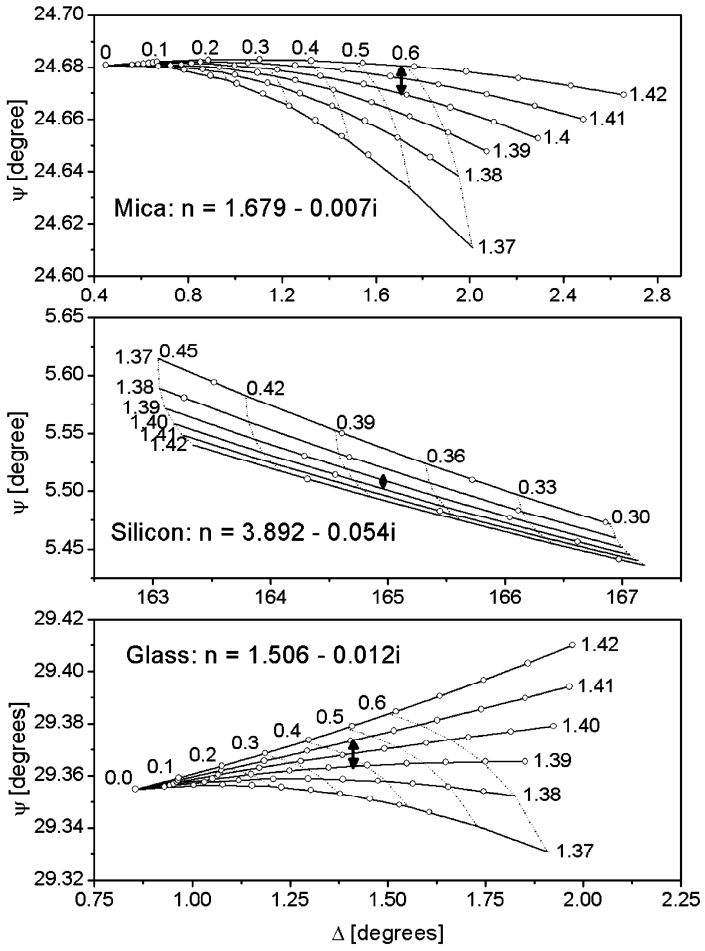


Figure 10. Simulations of measurement error on silica, mica and glass surface. Plotted are calculated ellipsometry readout parameters Δ and Ψ for phospholipid layers with refractive indexes ranging from 1.37 to 1.42 and with total adsorbed mass ranging from 0 to 0.6 ug/cm^2 for mica and glass surfaces and from 0.3 to 0.45 ug/cm^2 for the silicon surface [43]. Lines of equal mass are shown and the magnitude of experimental error is indicated by arrow heads. Data from Benes 2004.

The influence of experimental error on obtained values of d, n and Γ is shown in figure 10. Whereas on glass such error could cause error in Γ, it is shown that this is not so for silicon oxide, with mica somewhere in between.

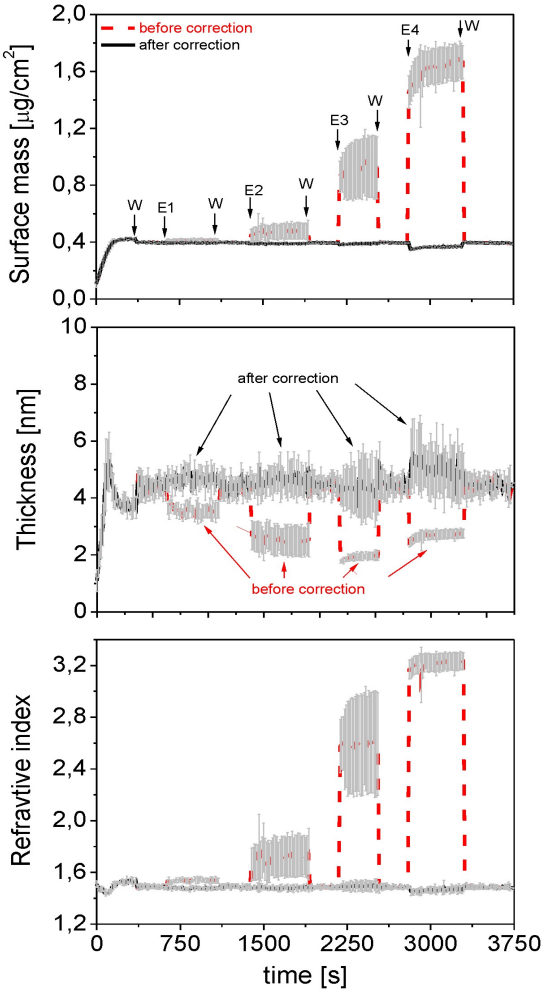


Figure 11. Thickness, refractive index and surface mass of DOPC/DOPS bilayer after addition of ethanol. Properly determined values, with n_1 values corrected for the presence of ethanol are shown as solid lines. "E1", "E2", "E3" and "E4" in the graph indicate addition of ethanol, 1.6, 3.2, 6.2, and 11.7 vol%, respectively. "W" in the graph indicate flushing with pure water. Artefactual results, calculated with a fixed refractive index n_1=1.33211of pure water are shown as dashed lines. Data obtained by author.

A last significant factor that causes error in ellipsometric results is the refractive index of buffer n_1. Incorrect values of n_1 used for calculation can yield totally wrong results. An example of this latter error was shown in a study of ethanol-induced so called "interdigitation" of SPBs on silica surfaces. Such interdigitation, that is, mixing of the hydrocarbon chains of opposite monolayers into a single layer with a corresponding lowering of membrane thickness, has been demonstrated in free-standing phospholipid double layers in solution [55]. We tried to verify this effect for SPBs and it was shown that use of a fixed refractive index of pure water (n_1= 1.33211) instead of correct values of water/ethanol mixtures (between 1.33306 to 1.33959) gives a false interdigitation

phenomenon (figure 11) [55]. The obtained values of refractive index of the layer (higher than 2.0) and surface mass (increased by a factor of 4) are much too large to be physically possible for organic substances.

Conclusions

The first chapter demonstrates that, in contrast to free-standing membranes, SPBs formed on silica surfaces do not show ethanol-induced interdigitation. In addition, the errors involved in ellipsometry are discussed. Surface mass of confluent DOPS/DOPC bilayers, as determined by ellipsometry, is approximately 0.4 $\mu g/cm^2$ (with error of ~1% of the bilayer); the thickness is about 6 nm (error from 0.1 to 1 nm - depending on the reflecting surface); and refractive index is 1.40 (with error 0.001 to 0.01). It is also demonstrated that ellipsometry allows accurate determination of the refractieve index of the buffer and that calculated thickness and refractive index of the membranes are very sensitive to error in this refractive index.

2. Combination of ellipsometry, laser scanning microscopy and Z-scan FCS elucidating interactions of antimicrobial peptides with model membranes

The following chapter brings an overview on two microscopic techniques: Laser Scanning Microscopy and Z-scan Fluorescence Correlation Spectroscopy (Z-scan FCS). These methods are introduced as suitable techniques used to visualize inhomogeneities in bilayers as well as to measure diffusion properties of phospholipids. Moreover these techniques are combined with ellipsometry to study the mechanism of the interactions of antimicrobial peptides with supported phospholipids bilayers.

2.1. Principles of fluorescence microscopy – Laser Scanning Microscopy and Z-Scan Fluorescence Correlation Spectroscopy (FCS)

2.1.1. Confocal microscopy setup (Laser Scanning Microscopy)

Confocal fluorescence microscopy is one of the most widely used microscopic techniques in biological sciences. The setup of a conventional confocal fluorescence microscope is shown in figure 12. Initially the collimated laser beam (excitation light) is reflected by the dichroic mirror and focused into the sample by a water- or oil- immersion objective. The dichroic mirror is reflective at the wavelength of the laser and transmissive at the wavelength of the fluorescence emission of the sample. The fluorescence emission from the sample is then collected by the same objective, passes the dichroic mirror and emission filter (which eliminates the rest of the excitation light transmitted through the dichroic mirror) and is focused into a pinhole, which is a circular aperture of a diameter in the range from 30 to 100 mm, allowing the fluorescence light (from the focal plane of the objective) to reach the detector.

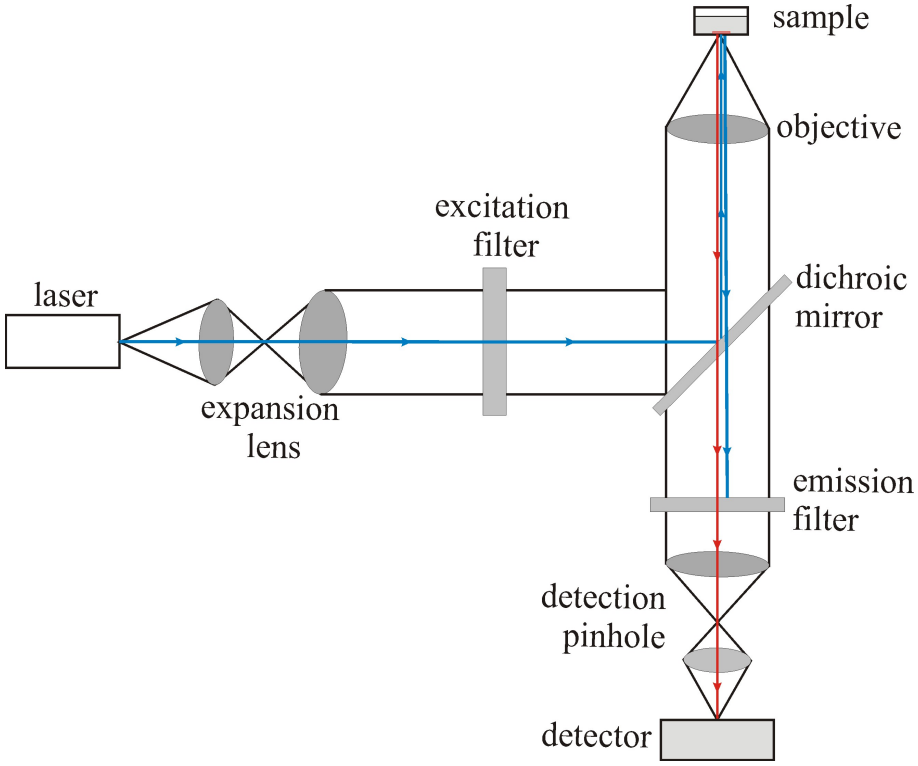


Figure 12. Confocal Microscopy setup

The fluorescence emission is collected from a small volume element of the sample. The size of the volume element is typically about 1 μm^3 or smaller [56-58]. The radius within the focal plane (usually denoted as *xy* plane) is diffraction limited to 200 to 300 nm, while its characteristic dimension along the axis of the microscope (the *z* axis) is a few micrometers [57-63]. The size and shape of this effective detection volume is given by the so-called point-spread function, which is the product of the excitation-light-intensity distribution within the sample and of the light-collection efficiency, which is determined by the detection optics (especially by the confocal aperture) [57, 58, 64]. The profile of the laser beam within the sample is Gaussian in the *x* and the *y* directions and Lorentzian in the *z* direction, however the shape of the effective detection volume is often approximated by a three-dimensional Gaussian shape [57, 65, 66]. The resultant image is then formed by scanning the sample with the focus of the microscope and thus collecting emission from different locations within the sample.

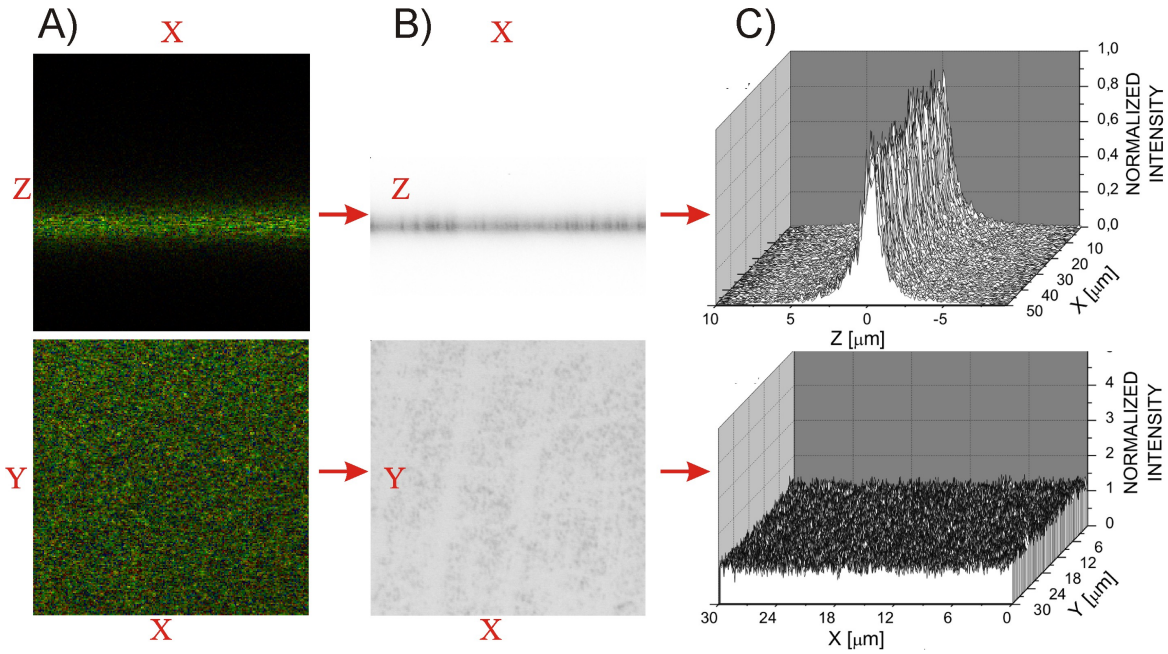


Figure 13. Original pictures from the confocal microscopy (A), normalized pictures to the maximum of intensity (B) and normalized fluorescence intensity profiles (C) of SPBs on mica formed from DOPC/DOPS (4:1) lipids and labelled with fluorescence lipid analogue Oregon Green 488 DHPE (in ratio 1:10000) recorded by confocal fluorescence microscope. The size of X/Y scans was 30 x 30 um (400x400 pixels) and that of X/Z scans, 50 x 20 um (400x200 pixels); each pixels was recorded for 1.2 ms. X/Z scans were started 10 um above the bilayer. Data obtained by author.

The sample (i.e. supported phospholipid bilayers) immersed in a cuvette with aqueous solution (buffer) is located within the plane perpendicular to the optical axis of the

microscope (X/Y plane). The membrane can be formed directly on the bottom of the cuvette, which is made of a transparent support (mica or glass) in order to let the laser beam illuminate the sample allowing, thus, imaging of the bilayer. The original confocal images of the bilayer in the plane perpendicular (X/Z) and parallel (X/Y) to the bilayer plane are shown in figure 13. The pixels include information on intensity and average lifetime of fluorescence in individual spots of the sample. The brightness of each pixel corresponds to the fluorescence intensity and the colour encodes average lifetime (red colour corresponds to the longest and blue colour to the shortest lifetime). Each image is scaled automatically to use the full colour and brightness scale. Such scaling, however, makes visual comparison of scans problematic, because the same levels of brightness or the same hues of colour represent different values of fluorescence intensity and lifetime. It would be, therefore, difficult to judge from such images for example the degree of homogeneity of a bilayer. Any minor heterogeneity in an otherwise smooth and homogeneous bilayer would appear as bright as fibrils or large lipid aggregates (the intensity of which is several times the intensity of the bilayer), which are for example observed in bilayers treated with membrane-active peptides. To overcome this drawback, rescaling all microscopic scans and converting them to greyscale (darkest shade corresponding to highest fluorescence intensity) is needed. This procedure discards the lifetime information, which is redundant for the analysis. The same scaling, then, applies to all images from a whole series of experiments facilitating their visual comparison (figure 13B). The normalized scans can be also shown in the form of fluorescence profiles (figure 13C), which allow visual quantitative estimation of the magnitude of changes in fluorescence intensity.

For non transparent support (like silicon), the setup analogous to a previously describe one [60] can be used (Figure 14). In this setup the sample is immersed in the cuvette by sample holder in the small distance (about the thickness of a cover glass) above the bottom of the cuvette and positioned parallel to it [60]. In this system the flushing system and stirrer can be installed as well, but stirring will be rather ineffective.

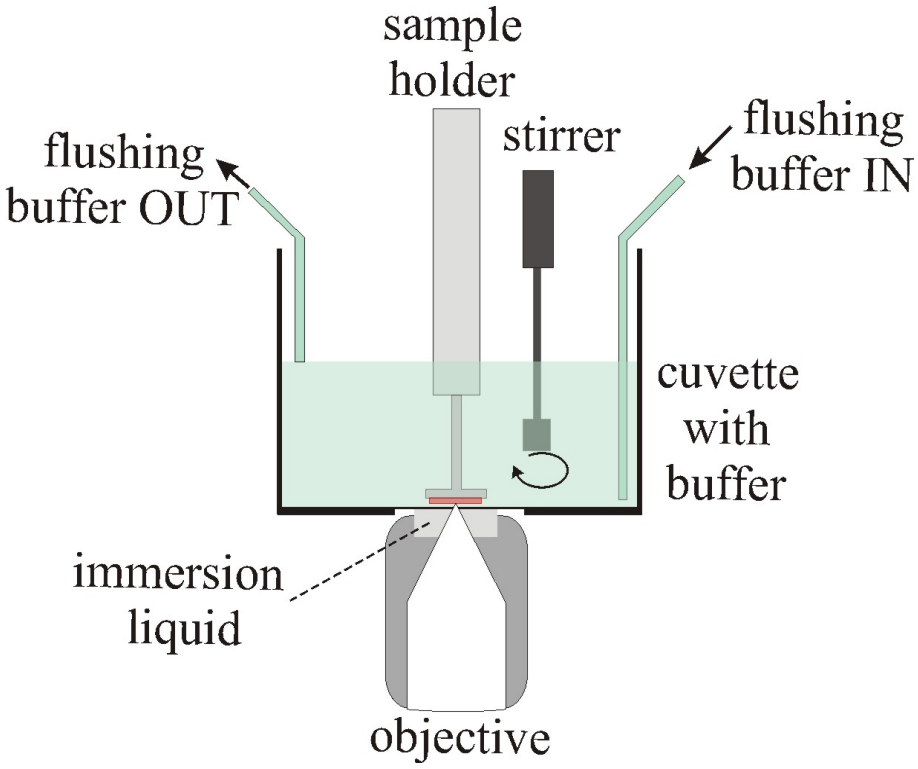


Figure 14. Scheme of sample holder for microscopy experiments

2.1.2. Z-scan Fluorescence Correlation Spectroscopy

Fluorescence correlation spectroscopy (FCS) is a common method used to characterize the diffusion properties of fluorescence species (e.g. Fluorescence phospholipid analogues in biological membranes [67-71], giant unilamellar vesicles [51, 72-77] or supported phospholipid bilayers [52, 56, 66, 69, 78, 79]). The method developed in the early 1970s [80-83], became widespread when the sensitivity of the method was increased by application of lasers with high temporal stability, single-photon detectors with low noise (usually a single-photon counting photomultiplier tube or a single photon avalanche diode) and confocal fluorescence microscopy with high-quality objectives, which is the experimental setup used most frequently nowadays [57, 58, 84]. In case of confocal FCS, the focal volume, from which fluorescence is collected, is the same as described in the previous section.

FCS is based on recording time traces of fluorescence intensity $I(t)$ with high temporal resolution and calculating their normalized autocorrelation function $G(\tau)$, which measures probability of detecting a photon at time $t + \tau$ if a photon was detected at time t.

$$G(\tau) = \frac{\langle I(t)\, I(t+\tau)\rangle}{\langle I(t)\rangle^2}, \tag{12}$$

where pointed brackets represent averaging over all values of *t*. The shape of the autocorrelation function is given by the timescale of fluctuations of fluorescence intensity *I*(*t*) originating from the detection volume. The fluctuations of fluorescence intensity are caused mainly by crossing of molecules in and out of the focal volume due to translational diffusion and happen usually on a millisecond to second timescale [58]. If more processes happen on comparable timescale, it is difficult to distinguish their contributions to the decay of the autocorrelation function (figure 15).

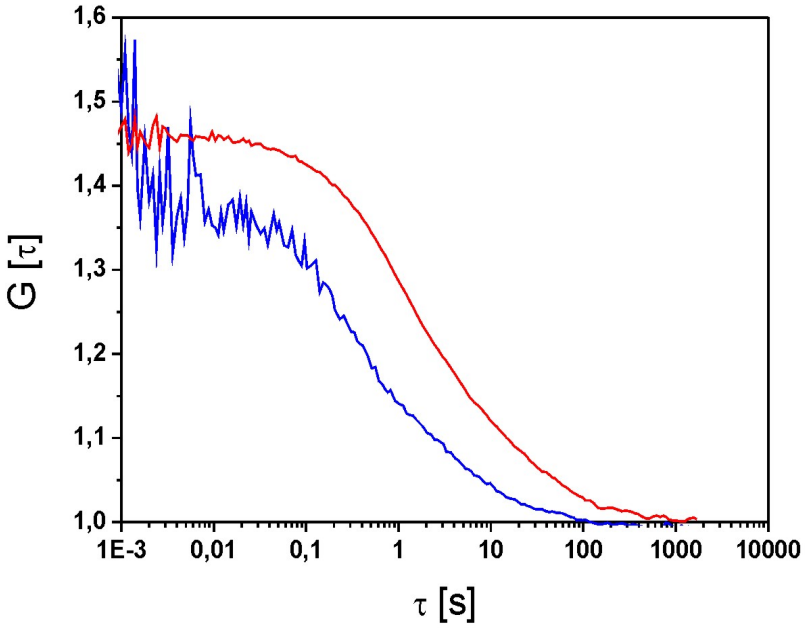


Figure 15. Autocorrelation functions of two different SPBs. Red curves correspond to SPB formed from DOPC/DOPS (4:1) lipids labelled with Oregon Green 488 DHPE (1:100000) on mica surface. Blue curve correspond to SPB formed from POPC/POPG (7:3) lipids and labelled with β-Bodipy 500/510 C_{12}-HPC (1:150000) on glass surface. Data obtained by author.

The autocorrelation function $G(\tau)$ (figure 14) for a three dimensional Brownian diffusion in a Gaussian volume element is given by equation (13) [84]

$$G(\tau) = 1 + \frac{\gamma}{PN}\frac{1}{1+(\tau/\tau_D)}\left(\frac{1}{1+(\tau/\tau_D)(\omega_0/\omega_z)}\right)^{1/2}, \tag{13}$$

where ω_0 and ω_z are characteristic dimensions of the detection volume in *xy* plane and along the optical axis respectively defined as distances at which the intensity drops by the

factor $1/e^2$. τ_D is the diffusion time and *PN* is the particle number (number of fluorescent particles within the detection volume). Correction factor γ is defined by Thompson [84] to take into account intensity profile in the focus and depends on experimental geometry (for three dimensional Gaussian profile it equals $2^{-3/2}$ and 0.5 for two dimensional). The dimension of the detection volume can be determined by a measurement of diffusion of a molecule with known diffusion coefficient.

When the diffusion is restricted to two dimensions (e.g. phospholipids bilayers and other planar systems) the expression for autocorrelation function is simplified to the following form [84]

$$G(\tau)_{2\mathbf{D}} = 1 + \frac{\gamma}{PN}\frac{1}{1+(\tau/\tau_D)}. \qquad (14)$$

To account for intersystem crossing, an average fraction of fluorophores in triplet state *T* and intersystem crossing relaxation time τ_T need to be induced into the equation (14):[85]

$$G(\tau)_{2\mathbf{D}T} = 1 + \left[1 - T + T\exp(-\tau/\tau_T)\right]\frac{\gamma}{PN(1-T)}\frac{1}{1+(\tau/\tau_D)}. \qquad (15)$$

The physically relevant parameters τ_D and *PN* can be then extracted from the experimentally obtained autocorrelation function $G(\tau)$ via nonlinear fitting with an appropriate theoretical model (equations 13 – 15). Due to the highly non-linear connection between the physically relevant parameters and the measured autocorrelation function, it is very difficult to analyse the accuracy of their estimation [59]. The standard deviation of the fit of the autocorrelation curve can be obtained using the method described by Wohland et al. [86].

Another artefact, which can influence the results of FCS is caused by deviations of the real shape of the detection volume from its form assumed in derivation of above given theoretical models of diffusion coefficient. A detail discussion of the sources of those artifacts (like laser-beam astigmatism, refractive-index mismatch between the sample and the objective's immersion medium or imperfect pinhole adjustment) and numerical simulations showing how they influence the physically relevant parameters obtained by FCS (τ_D and *PN*) are presented in contributions of Jörg Enderlein and his group [57, 58, 64, 87, 88].

The most important source of artifacts in the case of FCS in planar systems (e.g. phospholipid bilayers) is the problem with positioning the sample with respect to the focus along the *z* axis. The thickness of a SPB is about 7 nm and therefore several orders of magnitude smaller than the characteristic dimension ω_z of the detection volume. Different positions of sample with respect to the focus result in different diameter of illuminated area and thus in different measured values of diffusion time τ_D and particle number *PN*.

There are few ways how to overcome the problem of positioning the samples. The most recent method is two-focus FCS [65, 79, 89], which requires a non-standard set-up using two alternatively pulsed polarized lasers. Another is the "*Z*-scan" method [51, 66, 69]. This method has the advantage that can be easily performed with a standard FCS setup. It should be pointed out, that this method is the only artifact-free single focus measurement of lateral diffusion coefficients [66]. Numerical simulations have further proved that it is free of the usual artifacts of conventional FCS techniques [65].

The principle of this method is based on measuring fluorescence autocorrelation functions $G(\tau)$ at different positions of bilayer along the z axis (with step-size typically 200nm), thus changing the distance Δ_z between the bilayer and the focus of the microscope. The dependencies of diffusion time τ_D and particle number *PN* on Δ_z have parabolic character (figure 16) and can be described by following equations [66, 90, 91]:

$$\tau_D(z) = \frac{\omega_0^2}{4D}\left(1 + \frac{\lambda_0^2 \Delta_z^2}{\pi^2 \omega_0^2}\right), \tag{16}$$

$$\tau_D(z) = \pi c\, \omega_0^2\left(1 + \frac{\lambda_0^2 \Delta_z^2}{\pi^2 \omega_0^2}\right), \tag{17}$$

where *D* is the lateral diffusion coefficient of the fluorescent molecule in the phospholipid bilayer, ω_0 is the radius of the excitation beam in the plane of focus, *c* is the surface concentration of diffusing fluorescent molecules and λ is the wavelength of the excitation light in the medium of the sample.

It has to be pointed out that in the figure 16 the maximum of total countrate is shifted to about 800 nm to the left (to the buffer side), because in buffer is more intensity than in the surface. Thus the measuring in the place of the highest intensity would be out of focus [66].

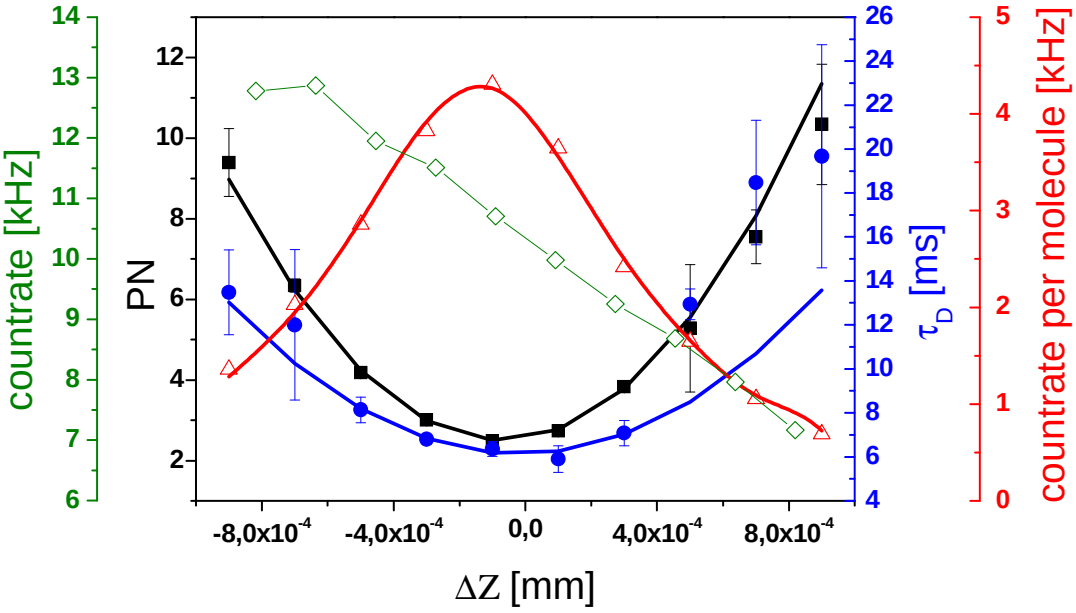


Figure 16. Dependences of diffusion time τ_D (-●-), particle number PN (-■-), countrate per molecule (-Δ-) and total countrate (fluorescence intensity) (-◊-) on the sample position ΔZ for SPBs (made from POPC/POPG (7:3) labeled with b-Bodipy 500/510 C_{12}-HPC (1:150000) on glass surface). Data obtained by author.

Autocorrelation functions measured for different *z* positions are fitted with equation (14) or (15) and obtained parameters PN_z and τ_{Dz} are plotted against *z* (figure 17). Fitting those dependencies with equations (16) and (17) yields directly the following parameters: lateral diffusion coefficient *D* of the studied molecule within the phospholipids bilayer; surface concentration *c* of the molecule within the bilayer and the radius of the excitation beam in the focus ω_0. The great advantage of this method is that it gives absolute values of searched parameters, independent on external calibration [66].

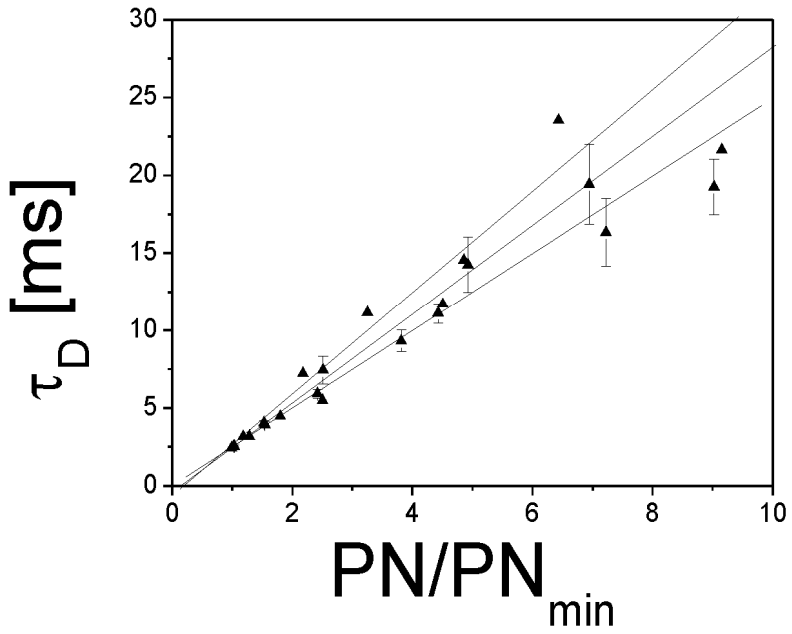


Figure 17. The plot shows the diffusion time (τ_D) versus particle number (PN/PN_{min}) measured at different Z positions of the focal plane with respect to the bilayer. Measurements were performed for three different bilayers made from DOPC/DOPS (4:1) lipids labelled with Oregon Green 488 DHPE (1:100000) on mica surface. The measurement points were linearly fitted and fits for individual points are shown in the plot. From the fitting of these lines we can calculate diffusion coefficients and the surface concentrations of the molecules within the bilayer; from the cross with Y axis the intercept. Data from Miszta 2007

2.1.3. Requirements for detection of supported phospholipid bilayers

If we want to visualize supported phospholipid bilayers by confocal microscopy we have to use fluorescence chromophores. These fluorescence phospholipid analogues have to be first mixed together with normal phospholipids molecules and sonicated together to form the vesicles. After formation of SPBs in a cuvette from these vesicles the bilayer will contain the fluorescence analogues in both leaflets of the SPBs. The labeling ratios for microscopy imaging are usually quite high to maximalize signal to noise ratio without affecting the properties of the bilayer dramatically (for example the group of Paavo Kinnunen used ratio 1:50 [92-94] Burns et al. [95] ratio 1:200 and Chiantia et al. [78] used ratio 1:1000). In Z-scan FCS the situation is different. The signal to noise ratio is the highest when there is on average about one fluorescent molecule within the detection volume [66, 85]. This means that the concentrations of fluorescent molecules (fluorescently labeled lipid

analogues, peptides or proteins, whose mobility in an SPB is studied) have to be rather low for performing FCS. For example Benda et al. [66] found the optimal ratio of labeled to unlabeled phospholipid molecules to be $1:5\cdot10^5$; Przybylo et al. [51] used the ratio $1:2\cdot10^5$; Chiantia et al. [78] the ratio $1:2\cdot10^4$ and Forstner et al. [96] used also the ratio $1:2\cdot10^4$.

During the measurement we have to remember that the thickness of SPBs is typically about 5 nm [97-99] and therefore negligible comparing to the size of the effective detection volume in *z* direction and many lateral inhomogeneities in the bilayer can be about an order of magnitude smaller than the diameter of the detection volume in *xy* plane. Thus a homogeneous appearance of the scan of the SPBs in *xy* plane does not necessarily mean a perfectly homogeneous bilayer. It is important to notice that from the appearance of a scan in a plane perpendicular to the plane of the support is difficult to distinguish from the whether a supported bilayer or an adsorbed vesicular layer or a bilayer with vesicular layer adsorbed on top of it was formed. The information concerning the quality of the SPB can be obtained by scanning a smaller area with high excitation intensity resulting in photobleaching in the area. If a bilayer had been formed, the fluorescence intensity would recover due to free diffusion of fluorophores from other parts of the bilayer (principle of the method of fluorescence recovery after photobleaching – FRAP), while vesicles have no source of unbleached fluorophores.

Although the confocal microscopy is not a perfect method for studies small changes in the bilayer structure (such as pore formation) because the resolution of the microscopy is limited to 200-300 nm, it is sufficient technique to visualize any larger structures (in range of micrometers) like amyloid-like fibers [93, 100] or tubular lipid protrusion [92, 101]. Moreover when fluorescently labeled peptide molecules are used, it can be used to study localization of peptide within different lipid structures [92, 93]. Because the fluorescence intensity from a unit area of a bilayer is proportional to the number of fluorescently labeled molecules within that area, which is again proportional to the total number of lipid molecules, we can conclyde from a decrease in fluorescence intensity that some lipid molecules were removed from the bilayer (for example, because of thinning and spreading of the bilayer or micellization caused by the peptide). In this type of experiments care is needed because decrease of intensity can be also caused by quenching of fluorophore by the peptide molecules or by changes in hydration of the bilayer in the fluorophore's vicinity [102] and an independent estimation of the effects of peptide on the fluorophore is needed.

2.2. Antimicrobial peptides

Antibacterial peptides are a large and varied group of peptides produced by the innate immune systems in virtually all multi-cellular organisms (e.g., single-celled microorganisms, insects and other invertebrates, plants, amphibians, birds, fish, and mammals, including humans) [103-105]. In many cases, their primary role is killing invading pathogenic organisms; however, they can also act as modulators of the innate immune response in higher organisms [105-112]. These are mostly amphiphilic molecules due to the spatial segregation of hydrophobic and cationic amino acid residues with an electropositive charge of at least +2 [103, 104]. Activities of antibacterial peptides differ both within and between distinct structural peptide classes [103, 107-109, 113, 114]. Antimicrobial peptides have been extensively investigated for potential applications as food preservatives, antiseptic agents and antibiotics, against which microbes develop little resistance, or as potential anti-tumor agents [103, 115-119]. Nevertheless, questions concerning the exact mechanism of AMPs' have not been fully answered yet.

The main factor in the selectivity of antimicrobial peptides for bacterial cells over eukaryotic cells represent negatively charged components present at the outer bacterial membrane, such as negatively charged phospholipids, however some lytic effect has been found also in the case of zwitterionic lipids [113, 117, 120-123]. The mechanisms of interactions of antimicrobial peptides with viral, bacterial, or fungal membranes can be divided in two general groups, either membrane-permeabilizing or non-membrane-permeabilizing mechanisms.

In the first group are peptides that directly interact with membranes and cause three types of events: formation of transient channels, micellarization, or dissolution of the membrane. Many different models were proposed (barrel-stave, carpet, detergent, toroidal pore, aggregate models, and fibrils formation) to explain those mechanisms [92, 110-112, 124, 125]. To this group belong peptides, which are the prototypicals linear and adopt α-helical conformation in contact with hydrophobic side of membranes. At low concentrations these peptides align predominantly parallel to the membrane surface. Increasing peptide concentration the orientation of peptides changes to transmembrane or pseudo-transmembrane orientation. The most investigated α-helical antimicrobial peptides are Melittin from the venom of European honeybee (*Apis mellifera*) [126-128] and Magainin 2 from the skin of the African frog *Xenopus laevis* [104, 129-131].

Peptides from the second group can translocate across the membrane into the cytoplasm without causing major membrane disruption [132-136]. These peptides often called "defensins" have relatively rigid secondary structure of three β–strands and can inhibit nucleic acid synthesis, protein synthesis, enzymatic activity, and cell wall synthesis [103, 134, 135, 137]. One of the most bactericidal defensin produce by mouse Paneth cells (*Mus musculus*) is Cryptdin-4 (Crp-4) [123, 134, 138]. Mechanism of interactions of Crp-4 (as a example of β–strands peptide) with supported phospholipid bilayers is discussed in next section.

2.3. Interactions of antimicrobial peptides with model membrane – combination of ellipsometry and fluorescence microscopy *(Paper II and Paper III)*

In the following paragraph the ellipsometric and fluorescence microscopy approaches are combined to demonstrate the mechanism of antimicrobial peptide interactions with supported phospholipid bilayers. The chosen methods complement each other in several aspects including spatial and temporal resolution. Ellipsometry is a suitable technique to provide the information on association of peptides with SPBs and the mode of binding of peptides molecules to the bilayers (peripheral or integral). These information's can be deduced from the calculated parameters of adsorbed layer (thickness, refractive index which is related to the density of the layer and surface mass) with very good precision. Confocal Laser Scanning Microscopy on the other hand, is among the techniques perfect for visualization of lateral inhomogeneities of the bilayer, their size, shape, and distribution. When the peptide binds to the membrane without causing any significant loss of lipids and the membrane remains continuous, Z-scan FCS can be performed to describe the mobility of the lipids in the bilayer.

2.3.1. Interaction of Cryptidin-4 and Magainin 2 with SPBs (Paper II)

In the present section the ellipsometry was combined with microscopic techniques to characterize changes of SPBs induced by the antimicrobial peptides cryptdin-4 and magainin 2. The Cryptdin-4, a triple-stranded, β-sheet defensine, interact with a phospholipid bilayer in a different manner than magainin 2, a prototypical linear AMP that

adopts an α-helical structure in membrane mimetic environments [50]. Some studies suggest that Magainin 2 acts via pore formation or via carpet model [111, 130, 139], while Cryptdin-4 binds and permeabilizes model membranes by a transient, graded leakage mechanism and does not insert as deep into the membrane as the α-helical peptides [135, 136, 140, 141].

Fluorescence intensity scans of the bilayer before and after application of peptides (cryptdin-4 and magainin 2) and after flushing with buffer present Figure 18 and 19. These scans were normalized to the maximum of intensity before peptide addition (X/Z scans) and to the average intensity before peptide addition (X/Y scans). Scans of pure SPBs prior to treatment with peptide show that the bilayer was homogenous and confluent. After application of both peptides a decrease in fluorescence intensity is observed and the appearance of inhomogeneities in the lateral distribution of lipids. However, Crp-4 evoked a much smaller decrease in intensity and left the bilayer less perturbed. Flushing of both peptides leaded to a further decrease in intensity, perhaps due to removal of SPB inhomogeneities.

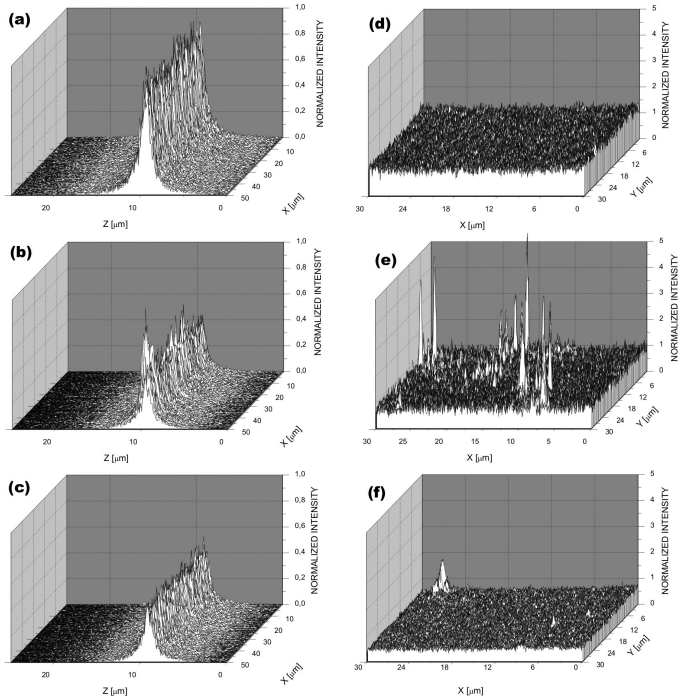


Figure 18. Normalized fluorescence intensity scans of SPBs on mica formed from DOPC/DOPS (4:1) lipids and labeled with fluorescence lipid analog Oregon Green 488 DHPE (1:10 000) before and after addition of Cryptdin-4 measured by confocal fluorescence microscopy. The size of X/Y scans was 30 x 30 um (400x400 pixels) and that of X/Z scans, 50 x 20 um (400x200 pixels); each pixels was recorded for 1.2 ms. X/Z scans were started 10 um above the bilayer. Figures (a) and (d) show pure SPB; figures (b) and (e) bilayer after treatment with peptide and figures (c) and (f) bilayer after final flushing. Data from Miszta 2007.

To estimate the extent of lipid loss induced by treatment with peptides, the changes of overall fluorescence intensities of the *X/Y* scans were calculated. It has to be pointed out that the fluorescence intensity due to quenching of the Oregon Green chromophore attached to the lipids by peptides decrease to 75% (experiments performed in steady-state measurements of bulk fluorescence intensity of a vesicular suspension) [50]. Thus, the fluorescence intensity after treatment with Crp-4 decreased to 72%, what means only minor loss of lipids from the bilayer, while lipid loss induced by magainin 2 (37% of original fluorescence intensity) is approximately 50% and significant. After flushing fluorescence intensity of the membrane pre-treated with Crp-4 decreased further to 50%, and for Magainin 2 to 24% of the original value (before peptide application). In case of cryptdin-4, flushing removed almost all lipid structures loosely bound to the bilayer (inhomogeneities in the intensity) and resulting bilayer appeared to be intact after the apparent lipid loss. For Magainin 2 however, the flushing did not remove these inhomogeneities.

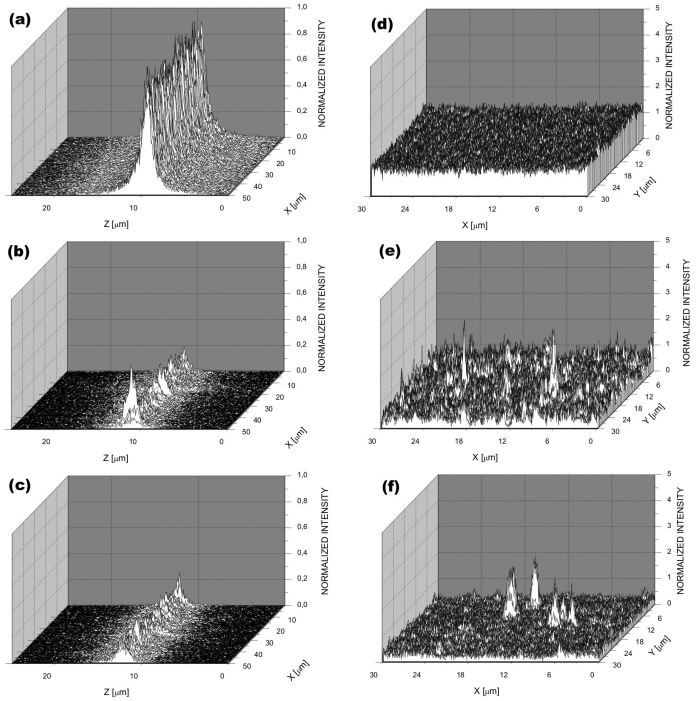


Figure 19. Normalized fluorescence intensity scans of SPBs on mica formed from DOPC/DOPS (4:1) lipids and labeled with fluorescence lipid analog Oregon Green 488 DHPE (1:10 000) before and after addition of Magainin 2 measured by confocal fluorescence microscopy. The size of X/Y scans was 30 x 30 um (400x400 pixels) and that of X/Z scans, 50 x 20 um (400x200 pixels); each pixels was recorded for 1.2 ms. X/Z scans were started 10 um above the bilayer. Figures (a) and (d) show pure SPB; figures (b) and (e) bilayer after treatment with peptide and figures (c) and (f) bilayer after final flushing. Data from Miszta 2007

Ellipsometric results performed for the same peptides are presented in the figure 20. These results show that after application of Crp-4 the surface mass increased without altered thickness and only minor change in refractive index, which indicates that the peptide binding does not significantly change the lipid structure. Flushing with buffer resulted in an immediate decrease in surface mass but still unaffected thickness and almost no refractive index. This may be due to removal of certain lipid inhomogeneities as indicated by the results of LSM (Figure 18) and possibly also some peptide molecules. Surface mass after flushing, however is slightly higher than its original value what indicates that not all peptide molecules were removed.

Magainin 2, however interacts with the membrane differently. A small decrease (approximately 10%) in surface mass and refractive index suggest that the density of the layer is lower and the relatively large loss of lipids deduced from LSM results is partially compensated by peptide adsorption. Moreover, decrease of surface mass caused by flushing is likely due to additional loss of lipids and peptide. The significant increase in adsorbed layer thickness after addition of Magainin 2 can be explained by formation of small lipid structures that protrude parallel from the SPB surface accompanied by thinning of the rest of the bilayer. These results are confirmed by work of Matsuzaki et al. who showed the formation of fibrillar structures induced by Magainin 2 [129]. Flushing with buffer caused decrease in thickness close to its original value, perhaps due to removal of protruding lipid structures, which is consistent with results of LSM (Figures 19) and decrease in surface mass (Figure 20).

Z-scan FCS results performed for Crp-4, clearly show that the lateral mobility of lipids within the bilayer is reduced by addition of peptide, as evident by the decrease in diffusion coefficient (Figure 21 and Table 2). In case of Magainin 2 the bilayer after application of peptide was not confluent, hence it was not possible to perform the Z-scan FCS experiments.

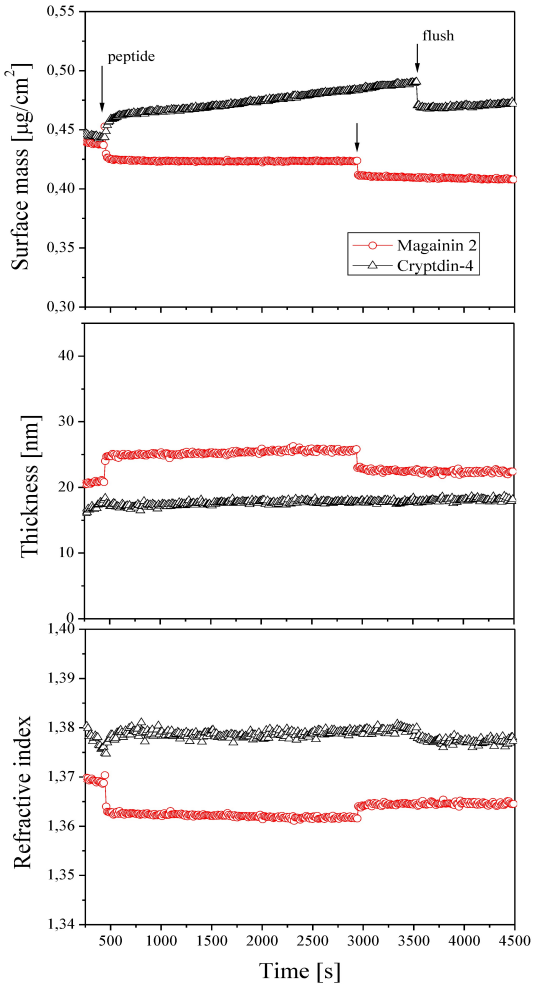


Figure 20. Surface mass, thickness and refractive index of DOPC/DOPS (4:1) bilayer adsorbed on silicon surface after addition of cryptrin-4 (-Δ-) and magainin 2 (-O-) measured by ellipsometry. "Peptide" in the plot indicates addition of peptide solution, and "flush" indicates flushing with fresh buffer. Data from Miszta 2007

The diffusion properties measured at different place in the SPB and larger differences in surface concentrations of fluorescent chromophore show that the bilayer is less homogenous (Figure 21 and Table 2). Changes induced by Crp-4 are partially reversed by flushing with buffer (perhaps due to only partial removal of peptide molecules from the bilayer) and the SPB again becomes more homogenous in agreement with LSM results. Moreover, after final flushing, the surface concentration of fluorescent molecules returned to the values prior to peptide addition. The intercept with the diffusion time (τ_D) axis is in all cases close to 0, meaning that the diffusion in the bilayer can be regarded as free and that there are no heterogeneities smaller than the optical resolution of microscope (~250 nm). It should be pointed out that the LSM experiments, or *Z*-scans at different *X/Y*

positions, and the z-scan at a certain position are complementary in terms of their resolution. The size of inhomogeneities observed in the first type of measurements is ~ 250 nm or larger. On the other hand, *Z*-scan FCS may provide information on heterogeneities smaller than ~ 250 nm [69, 142].

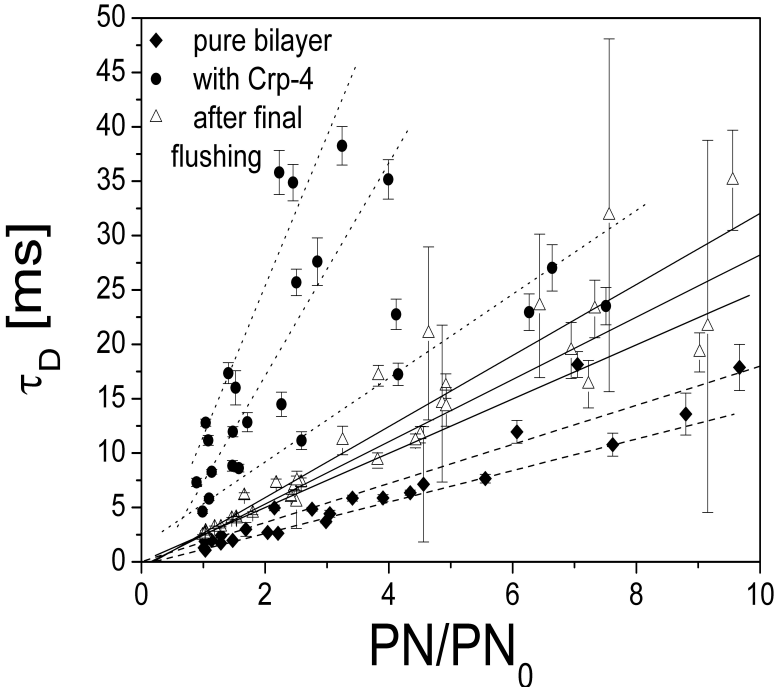


Figure 21. The plot shows the diffusion time versus particle number measured at various Z positions of the focal plane with respect to the bilayer. The measurements were performed at different points within pure bilayer (DOPC/DOPS (4:1)), after treatment with Cryptdin-4 and after flushing. These points were linearly fitted and fits for individual points are shown in the plot with standard errors. Data from Miszta 2007

Table 2. Parameters of DOPC/DOPS (4:1) bilayer labeled with Oregon Green 488 DHPE (1:100000) on mica surface before and after application of Cryptdin-4 calculated from Z-Scan FCS. Average values of surface concentration of fluorescence molecules C, effective diffusion D and the intercept of linear fit (with τ_D axis) τ_0 are shown with their standard errors. Data from Miszta 2007.

	Concentration		Diffusion coefficient		Intercept	
	C (pmol/m^2)	ΔC (pmol/m^2)	D (μm^2/s)	ΔD (μm^2/s)	τ_0 (ms)	$\Delta\tau_0$ (ms)
Pure membrane	30	5	7.5	1.5	-0.2	0.2
With cryptdin-4	40	10	2.0	0.2	0.7	2.0
After flushing	30	5	4.1	0.6	-0.3	0.3

Comparing both peptides, it seems that they interact with the supported phospholipid bilayers in different manner. Cryptdin-4 enters the bilayer without changing it thickness but making it more rigid. The peptide molecules are not removed by flushing the SPB, and the bilayer remains intact. Magainin 2 however, destroys the bilayer and forms with phospholipid the structures that protrude parallel to the surface. This is confirmed by a significant increase of thickness of SPBs and decrease of surface mass. These structures are removable by flushing, leaving the SPB largely damaged [50].

2.3.2. Formation of melittin-lipids fibrils (Paper III)

Melittin, is a much investigated α-helical antimicrobial and haemolytic peptide from the venom of European honeybee (*Apis mellifera*). Is responsible for permeation of the membrane via formation of pores, although micellization or detergent-like effects have been also reported [23, 130, 143]. Diameters of melittlin induced pores have been estimated in the range of 1-6 nm [144, 145].

In the present section fluoresecene techniques and ellipsometry were combined to characterize two effect of melittin on supported phospholipids bilayers. The first one is formation of pores in the SPB, which occupy approximately 40% of the bilayer. The second, simultaneous effect is the formation of tubules of approximately 30 nm radius and length of the order of 10 μm.

Figures 22 – 24 show the results of parallel LSM and ellipsometric experiments studying the temporal evolution of the SPBs after treatment with melittin. All the repetitions of the experiment included in the figures were performed in a low ionic strength buffer (20 mM HEPES and 0.1 mM EDTA) of pH = 6.9. For clarity's sake, each experiment may be divided into three stages denoted A, B and E (in agreement with the description of figure 22): the characterization of the initial SPB (stage A), monitoring of its temporal evolution after the addition of melittin (stage B) and characterization of the final state of the SPB, after stage B has been terminated by flushing the sample with excess of buffer (stage E). In this section the interpretation of those results in individual phases of the experiment is discussed.

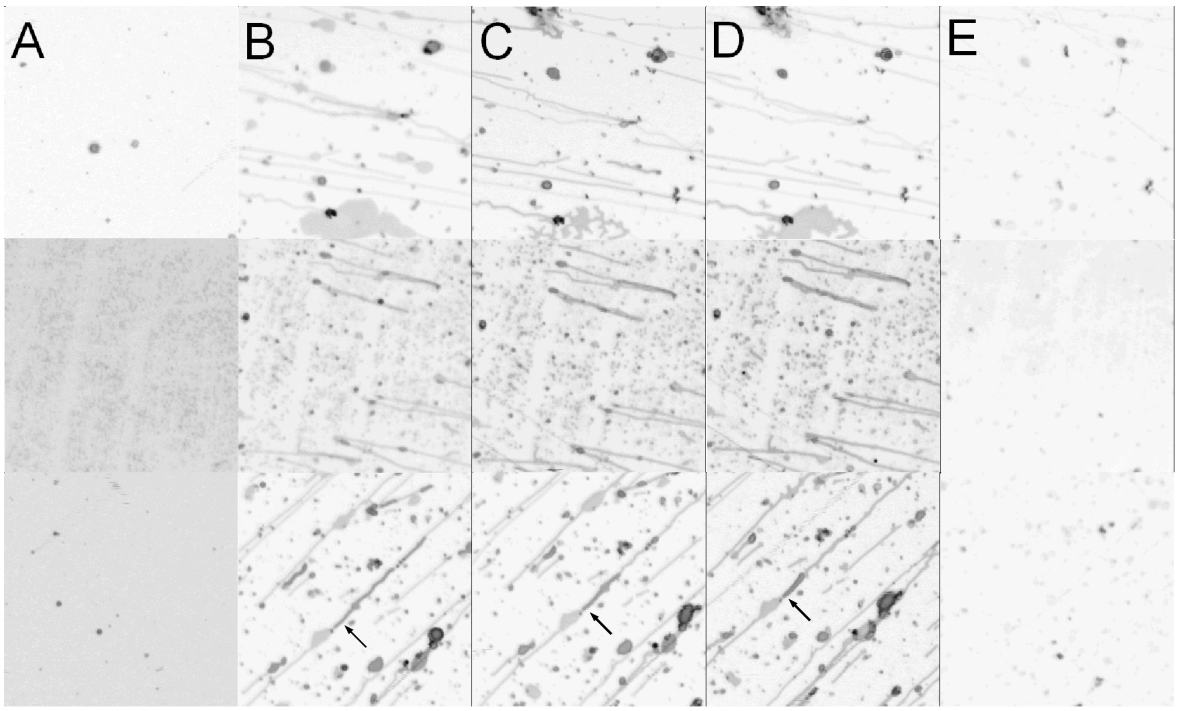


Figure 22. Fluorescence intensity scans (*X/Y* plane) of three different experiments showing the effect of melittin (1 μM) on SPBs (POPC/POPG 7/3) and its reproducibility. The size of the scans is 30 × 30 mm (300 × 300 pixels). SPBs before (A), 10 (B), 30 (C), 90(D) minutes after the treatment with peptide and after flushing with buffer (E) are shown. Scans were normalized to the maximum of intensity in each of the three series of measurements (the darkest shades correspond to the highest fluorescence intensity). All experiments were performed in buffer (pH = 6.9) containing 20 mM HEPES and 0.1 mM EDTA. Data from Machan 2009[146]

Stage A: Initial bilayers look regular and homogeneous in *XY* scans (Figure 22 A) and *XZ* scans (Figure 23 A) with only occasional spots of higher intensity, which consist most likely of unfused vesicles and their aggregates adsorbed to the surface. The mass of the initial SPB estimated by ellipsometry ranges between 0.3 and 0.4 μg/cm^2, which agrees with the values expected when considering the area per lipid between 0.6 and 0.7 nm^2. The lateral diffusion coefficient of the lipids in the SPB $D_0 = (4.5 \pm 1.0)$ μm^{2}s^{-1}.

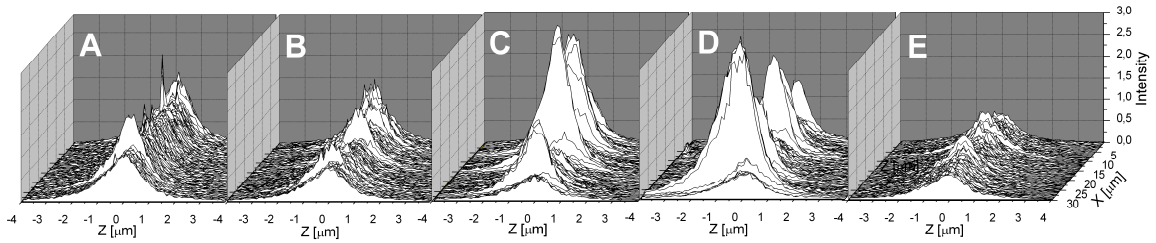


Figure 23. Normalized fluorescence intensity profiles (*X/Z* plane) showing the effect of Melittin (1µM) on SPBs (POPC/POPG 7/3). The size of the scans is 15 × 30 mm (300 × 300 pixels). SPBs before (A), 10 (B), 30 (C), 90(D) minutes after the treatment with peptide and after flushing with buffer (E) are shown. Scans were normalized to the average intensity at the position of the SPB (*Z* = 0) in the initial bilayer (A). Data from Machan 2009

Stage B: The ellipsometric results (Figure 24 A,B) show that the addition of melittin to the sample is immediately followed by a rapid loss of approximately 25 % of surface mass (≈ 0.1 µg/cm^2), reaching its full magnitude in 2 to 5 minutes. As expected for pore formation, the thickness remains unchanged like in the case of PLA2-induced degradation of SPBs, which has been shown by atomic force microscopy to result in patches of undisturbed bilayer with widening empty spaces in between [43, 147]. The loss of lipid surface mass is yet larger, because it is partly compensated by adsorption of melittin. The extend of the loss of lipids can be estimated from the decrease in intensity in LSM scans. For this purpose the *XZ* scans was used and integrated the cross sections of the intensity profiles; the values from several sections of the respective *XY* scans were then averaged. *XY* scans are less convenient, because their intensity depends on the exact position of the SPB with respect to the focus, which can slightly vary during the experiments.

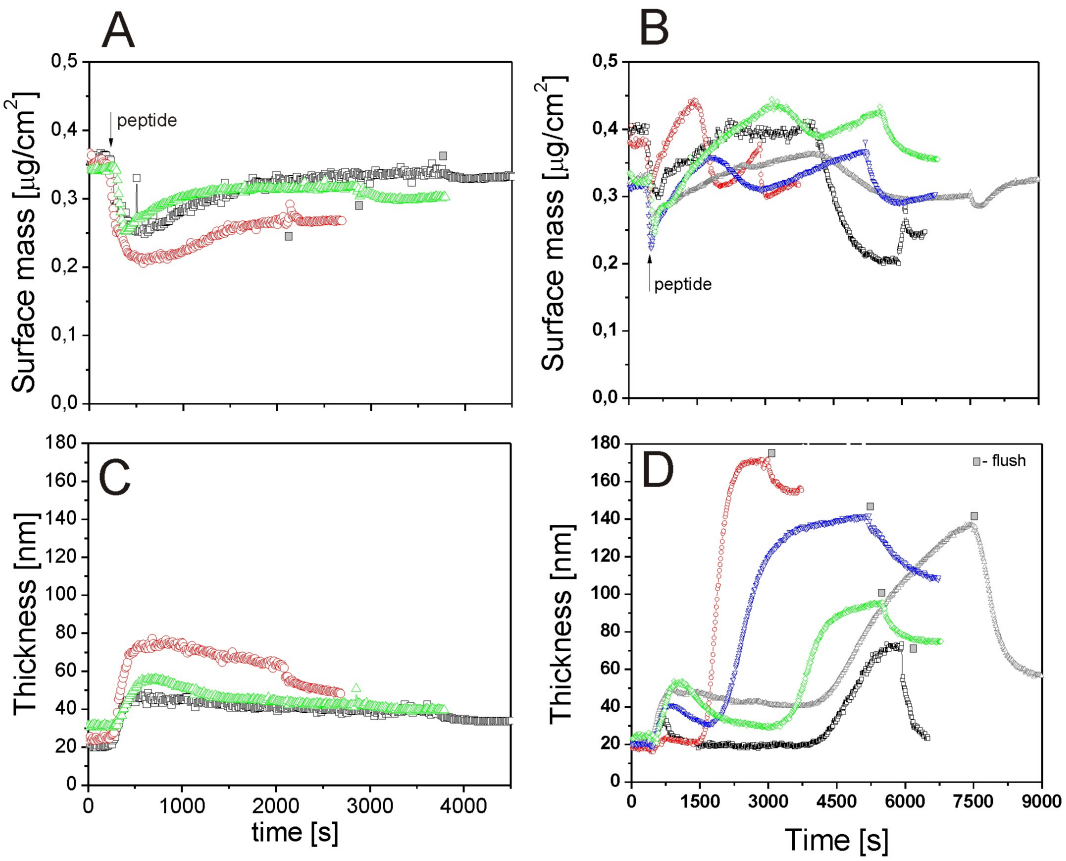


Figure 24. Temporal evolution of thickness (B,D) and surface mass (A,C) of SPBs (POPC/POPG 7:3) during the treatment with melittin (1 µM) and after the flushing with buffer measured by ellipsometry. Several repetitions of the experiment with fast (A,C) and slow (B,D) stirring rate are shown. All experiments were performed in buffer (pH = 6.9) containing 20 mM HEPES and 0.1 mM EDTA. Values were recorded every 12 – 14 s; the times when peptide was added (*peptide*) and when the sample was flushed with buffer (■) are indicated within the plots. Data from Machan 2009

As can be seen in the figure 23 B, the bilayer is no more homogeneous. If we exclude the structures of higher intensity from the analysis, we arrive to (54 ± 7) % of the initial fluorescence intensity. The influence of the presence of melittin on the intensity of the given fluorescent probe was checked in a bulk experiment with a suspension of SUVs of identical lipid composition and a 10 % quenching in intensity was found for 1 µM melittin. The loss of lipids from the bilayer is, thus, approximately 40 %. This means that the surface mass of melittin associated with the bilayer is approximately 0.06 µg/cm^2 (90 mmol/mol of lipids), a value consistent with the findings of Beschiaschvili and Seelig[121]. It can be conclude that the loss of lipid results from the formation of pores, which together occupy 40 % of the total surface area, although it is also possible that the total area of the pores is somewhat smaller and that the lipid density in the rest of the bilayer is reduced by the incorporation of the peptide molecules. The lipids removed from

the bilayer can be either pushed aside and into structures which protrude from the bilayer and are seen as the inhomogeneities in the *XY* scans (Figure 22 B, C, D) or released from the SPB most likely in the form of micelles, which may subsequently readsorb to form the observed inhomogeneities. If we do not exclude the mentioned inhomogeneities from the analysis of the intensity of *XZ* scans, we reach a value, which is approximately 80 % of the initial intensity, meaning that some lipid is indeed removed from the bilayer to the solution in the form of micelles. The initial loss of mass is followed by its partial recovery (starting within 5 minutes from the injection of the peptide). The increase is most likely caused by continuing adsorption of melittin, which may probably bind also to the leaflet of the SPB facing the support, which is known to be separated from the support by a thin layer of buffer[148, 149] and which has been made accessible through the pores. Other process contributing to the increase in mass can be the readsorption of some of the lipids released previously in the form of micelles.

The changes in mass are accompanied by an increase in thickness of the layer, which reaches a maximum within 10 minutes from the addition of melittin (the timescale of individual repetitions of the experiment varies probably due to variations in velocity of stirring). The thickness decreases, then, slightly until it reaches a stable value. The increase in thickness is clearly connected with the formation of the structures apparent in the *XY* scans (Figure 22 B, C, D). Note that the scans were recorded after the increase in thickness reached its maximum. These structures include long fibrilar ones similar to those observed by Domanov and Kinnunen, who concluded that they are microtubules growing out from the bilayer[92]. The tubules protrude from the SPB, their growth causing the rise in thickness, but the flow of the rapidly stirred buffer forces them to orientate themselves in one direction parallel to the surface of the SPB; the resulting thickness of the layer is, thus, approximately equal to the thickness of the SPB plus the diameter of the tubules. The tubules are stable within the time range of the experiment (that means in order of tens of minutes). The lipids within the tubules are mobile and, most likely, an exchange of lipids exists between the tubules and the bilayer, as indicated by a fast and complete fluorescence recovery after photobleaching (data not shown). When the intensity in XZ scans were integrated corresponding to the tubules (identified according to the *XY* scans), the average fluorescence intensity per tubule to be (43 ± 15) % of the initial fluorescence intensity was found. Considering the geometry of a cylindrical tubule placed above a planar bilayer within a Gaussian intensity profile of the radius ω_0 = (270 ± 30) nm (estimated by *Z*-scan

FCS), the radius of the tubule is (33 ± 9) nm, provided that the density of the lipids is the same as in the initial SPB. The thickness of the layer of tubules measured by ellipsometry is not more than 50 nm suggesting that the lipid density and, thus, the fluorescence intensity in the tubules is not reduced by the presence of melittin in comparison with the initial SPB. The total length of all tubules per 1 cm^2 is surprisingly high. Summing the length of tubules in the *XY* scans, we arrive to a total length of all tubules in the order of 10 m per 1 cm^2. Yet the mass of lipids forming the tubules (considering their radius to be less than 50 nm) is only in the range of a few per cent (not more than 10 %) of the total lipid in the sample. Apart from the tubules, small aggregates of vesicles or micelles and structures occupying larger area (an example can be found in the upper row of the figure 22 B, C and D) appear in the *XY* scans. We consider the latter type of structures to be bilayer stacks containing three bilayers, because its average fluorescence intensity (determined from *XZ* scans) is equal three times the intensity of the surrounding bilayer. The lateral diffusion coefficient of the lipids was reduced by the effects of the peptide to $D_1 = (2.5 \pm 0.5)\ \mu m^2 s^{-1}$, which are approximately 60 % of the initial value. The pores act as obstacles for the diffusion and reduce the diffusion coefficient by reducing the area accessible for lipid molecules [150]. The surface concentration of the fluorescently labelled molecule estimated by *Z*-scan FCS also decreased to about 60 % of its initial value, which is in a good agreement with the loss of lipids determined from the intensity of *XZ* scans.

Stage E: Flushing of the sample with excess of buffer results in removal of some of the inhomogeneities of the SPB; this is apparent from the *XY* scans (Figure 22 E) and it is demonstrated by a decrease in mass (about 0.07 $\mu g/cm^2$) and thickness in the ellipsometric results. The analysis of the fluorescence intensity of *XZ* scans yields a reduction in the total fluorescence intensity (and, hence, the total amount of lipids) to approximately 64%, while the intensity integrated with the exclusion of the inhomogeneities constitutes approximately 56 % of the initial value. The results of *Z*-scan FCS are supporting those findings; both diffusion coefficient of the lipids and the surface concentration of the fluorescent dye have remained essentially unchanged: $D_2 = (2.2 \pm 0.7)\ \mu m^2 s^{-1}$ and the surface concentration amounts about 55 % of its initial value. We can, therefore, conclude that the flushing with buffer led only to removal of some of the lipids forming the tubules and other inhomogeneities, while the pores remained in the bilayer unaltered. This is in contrast with our findings about the effects of peptide cryptdin-4 on SPBs, in which case

the decrease of diffusion coefficient was partially reversed after the sample had been flushed with buffer[50].

The flow of the buffer in the sample is certainly an important factor in the formation of the tubules. The force of the flow is responsible for the alignment of the tubules parallel to the surface and to the direction of the flow. Most likely, it is also one of the forces responsible for elongation of the tubules to their full length. Ellipsometric results from a series of experiments performed with a significantly slower stirring rate, demonstrate reproducibly another phenomenon (Figure 23 C, D). It is a large further growth of thickness to about 160 nm together with a temporary decrease in mass, which appears approximately 30 to 60 minutes after the injection of melittin to the sample (the onset of the effect varies between individual realizations of the experiment). The explanation can be a collapse of some of the tubules into much shorter and thicker multilamellar structures. Those are more rigid than unilamellar tubules and, thus, less prone to be bent by the force of the flow. Therefore, they protrude further into the solution forming a layer of high thickness and low density. The observed decrease in mass is probably a calculation artefact; tubules reaching too far from the surface may not be correctly included in the mass calculation, although the collapse of a tubule may be also accompanied by a small loss of lipids. Such collapses of tubules were occasionally observed in our LSM experiments (for example in the bottom row in figure 22 B, C, D; indicated by an arrow) and they have been also reported[92]. However, it would not be easy to gain more conclusive experimental evidence relating the large increase in thickness with collapse of tubules observed by microscopy. The size of the laser spot (and, thus, the area of the sample from which information was collected) was in the ellipsometric setup approximately 6 mm^2, which means almost 4 orders of magnitude larger than the size of our LSM scans. Therefore, even relatively rare phenomena can be reproducibly detected by ellipsometry, while the probability of their observation in a microscopic scan is very small. Furthermore, the LSM setup did not allow us to tune the stirring rate as exactly and reproducibly as in the ellipsometric setup making a more systematic study of the influence of the velocity of flow practically impossible.

Information available by ellipsometry is in several aspects complementary to that available by confocal fluorescence microscopy, especially in lateral and axial resolution. Axial resolution of a confocal microscope is in the order of μm, which is insufficient to detect changes in thickness caused by outgrowth protruding lipid structures such as the

melittin-induced tubules. Ellipsometry, on the other hand, lacks lateral resolution. LSM images are, therefore, for correct interpretation of the ellipsometric data on the evolution of thickness. The information on lateral mobility of lipids obtained by *Z*-scan FCS provides a valuable additional support for the interpretation. Although ellipsometry has the axial resolution in the order of 0.1 nm, the experimental data may suffer from systematic errors, which introduce a much larger inaccuracy to the results. Roughness of the solid support and imperfections of optical components of the ellipsometer can result in overestimation of measured thickness, refractive index and, hence, also mass, which may be the reason for variations of measured quantities between individual repetitions of the experiment (Figure 3). The initial values of thickness are in all repetitions rather high, suggesting they may suffer from systematic overestimation. Another possible explanation of that effect is the presence of a few unfused vesicles adsorbed to the bilayer or directly to the support, which make the layer appear thicker without increasing its mass significantly.

Conclusions

In this chapter, fluorescence microscopy techniques and the combination of these techniques with ellipsometry were used to acquire the information about the interactions of antimicrobial peptides with SPBs. The first study shows that Crp-4, a triple-stranded β-sheet peptide, interacts with phospholipid bilayers in different ways than magainin 2, a prototypical linear AMP that adopts an α-helical structure in membrane mimetic environments. The molecules of Crp-4 enter the bilayer without changing its thickness but by making it more rigid. The inserted peptide molecules are not removed completely by flushing with buffer, and the bilayer remains intact. On the other hand, magainin 2 causes a significant apparent increase of thickness of SPBs, and evidence from the subsequent study with melittin suggests that this results from formation of phospholipid structures that protrude from the bilayer surface. These structures are removed by flushing, leaving the SPB severely damaged. Further study of these observed differences in the interactions of Crp-4 and magainin 2 with phospholipid bilayers, for instance in terms of differences in the secondary structures, distribution of charge and aliphatic side chains, or different inherent flexibilities of the peptide backbones, is required.

The second study shows the effects of melittin on SPBs containing acidic phospholipids and the temporal evolution of those effects. Under all conditions used in the study, two reproducible effects were observed. The first one is rapid formation of pores in

the SPB, which occupy approximately 40 % of the bilayer. The second, simultaneous, effect is the formation of tubules of approximately 30 nm radius and length of the order of 10 μm. The force of the flow of the stirred buffer is probably one of the driving forces for the outgrowth and elongation of tubules and it also affects their stability. Flushing of the sample with excess of buffer removed most of the tubules, but did not affect the pores. Also, tubule formation required unphysiological low ionic strength of the buffer. We conclude, therefore that the formation of pores is probably more relevant for the biological activity of melittin than tubule formation.

References:

1. Tronstad L., *The validity of Drude's optical method of investigating transparent films on metals.* Trans. Far. Soc., 1935. **31**: p. 1151-1156.
2. Vroman, L., Lukosevicius, A., *Ellipsometric recordings of changes in optical thickness of adsorbed films, associated with surface activation of blood.* Nature, 1964. **2004**: p. 701-703.
3. Rothen, A., *The ellipsometer, an apparatus to measure thickness of thin surface films.* Rev. Sci. Instr., 1945. **16**: p. 26-30.
4. Rothen, A. and K. Landsteiner, *Serological reactions of protein films and denaturated proteins.* Journal of Experimental Medicine, 1942. **76**: p. 437-450.
5. Rothen, A., *Immunological reactions between films of antigen and antibody molecules.* J. Biol. Chem., 1947. **168**: p. 75-97.
6. Azzam, R.M.A.B., N. M., , *Ellipsometry and polarized light*. 1977, Amsterdam: Elsevier.
7. Mccrackin, F.L., et al., *Measurememt of Thickness and Refractive Index of Very Thin Films and Optical Properties of Surfaces by Ellipsometry.* Journal of Research of the National Bureau of Standards Section a-Physics and Chemistry, 1963. **A 67**(4): p. 363-&.
8. Holmström N., A.A., and Tengvall P.,, *In vitro studies on blood protein adsorption to gold and pyrolytic carbon at pre-set electrical potentials.* Coll. Surf. B., 1998. **11**: p. 265-271.
9. Speijer, H., et al., *Critical micelle concentrations and stirring are rate-limiting in the loss of lipid mass during membrane degradation by phospholipase A(2).* Biophysical Journal, 1996. **70**(5): p. 2239-2247.
10. Hermens, W.T., et al., *Effects of flow on solute exchange between fluids and supported biosurfaces.* Biotechnology and Applied Biochemistry, 2004. **39**: p. 277-284.
11. Cuypers, P.A., et al., *The Adsorption of Prothrombin to Phosphatidylserine Multilayers Quantitated by Ellipsometry.* Journal of Biological Chemistry, 1983. **258**(4): p. 2426-2431.
12. Streyer, L., *Biochemistry*. 4th ed., ed. W.H. Freeman. 2002.
13. Sackmann, E., *Supported membranes: Scientific and practical applications.* Science, 1996. **271**(5245): p. 43-48.
14. McKiernan, A.E., T.V. Ratto, and M.L. Longo, *Domain growth, shapes, and topology in cationic lipid bilayers on mica by fluorescence and atomic force microscopy.* Biophysical Journal, 2000. **79**(5): p. 2605-2615.
15. McConnell, H.M., et al., *Supported Planar Membranes in Studies of Cell-Cell Recognition in the Immune-System.* Biochimica Et Biophysica Acta, 1986. **864**(1): p. 95-106.
16. Brian, A.A. and H.M. Mcconnell, *Allogeneic Stimulation of Cyto-Toxic T-Cells by Supported Planar Membranes.* Proceedings of the National Academy of Sciences of the United States of America-Biological Sciences, 1984. **81**(19): p. 6159-6163.
17. Keller, C.A., et al., *Formation of supported membranes from vesicles.* Physical Review Letters, 2000. **84**(23): p. 5443-5446.
18. Starr, T.E. and N.L. Thompson, *Formation and characterization of planar phospholipid bilayers supported on TiO2 and SrTiO3 single crystals.* Langmuir, 2000. **16**(26): p. 10301-10308.

19. Richter, R.P., N. Maury, and A.R. Brisson, *On the effect of the solid support on the interleaflet distribution of lipids in supported lipid bilayers.* Langmuir, 2005. **21**(1): p. 299-304.
20. Grant, L.M. and F. Tiberg, *Normal and lateral forces between lipid covered solids in solution: Correlation with layer packing and structure.* Biophysical Journal, 2002. **82**(3): p. 1373-1385.
21. Heyse, S., et al., *Incorporation of rhodopsin in laterally structured supported membranes: Observation of transducin activation with spatially and time-resolved surface plasmon resonance.* Biochemistry, 1998. **37**(2): p. 507-522.
22. Srinivasan, M.P., et al., *Patterned supported bilayers on self-assembled monolayers: Confinement of adjacent mobile bilayers.* Langmuir, 2001. **17**(25): p. 7951-7954.
23. Steinem, C., H.J. Galla, and A. Janshoff, *Interaction of melittin with solid supported membranes.* Physical Chemistry Chemical Physics, 2000. **2**(20): p. 4580-4585.
24. Charitat, T., et al., *Adsorbed and free lipid bilayers at the solid-liquid interface.* European Physical Journal B, 1999. **8**(4): p. 583-593.
25. Tamm, L.K. and H.M. Mcconnell, *Supported Phospholipid-Bilayers.* Biophysical Journal, 1985. **47**(1): p. 105-113.
26. Csúcs, G. and J.J. Ramsden, *Interaction of phospholipid vesicles with smooth metal-oxide surfaces.* Biochimica et Biophysica Acta (BBA) - Biomembranes, 1998. **1369**(1): p. 61-70.
27. Kalb, E., S. Frey, and L.K. Tamm, *Formation of Supported Planar Bilayers by Fusion of Vesicles to Supported Phospholipid Monolayers.* Biochimica Et Biophysica Acta, 1992. **1103**(2): p. 307-316.
28. Mimms, L.T., et al., *Phospholipid vesicle formation and transmembrane protein incorporation using octyl glucoside.* Biochemistry, 1981. **20**(4): p. 833-840.
29. Roessner, C.A., D.K. Struck, and G.M. Ihler, *Injection of DNA into liposomes by bacteriophage lambda.* J. Biol. Chem., 1983. **258**(1): p. 643-648.
30. Axelrod, D., N.L. Thompson, and T.P. Burghardt, *Total Internal-Reflection Fluorescent Microscopy.* Journal of Microscopy-Oxford, 1983. **129**(Jan): p. 19-28.
31. Reviakine, I. and A. Brisson, *Formation of supported phospholipid bilayers from unilamellar vesicles investigated by atomic force microscopy.* Langmuir, 2000. **16**(4): p. 1806-1815.
32. Ratto, T.V. and M.L. Longo, *Obstructed diffusion in phase-separated supported lipid bilayers: A combined atomic force microscopy and fluorescence recovery after photobleaching approach.* Biophysical Journal, 2002. **83**(6): p. 3380-3392.
33. Richter, R.P. and A. Brisson, *Characterization of lipid bilayers and protein assemblies supported on rough surfaces by atomic force microscopy.* Langmuir, 2003. **19**(5): p. 1632-1640.
34. Richter, R., A. Mukhopadhyay, and A. Brisson, *Pathways of lipid vesicle deposition on solid surfaces: A combined QCM-D and AFM study.* Biophysical Journal, 2003. **85**(5): p. 3035-3047.
35. Andree, H.A.M., et al., *Binding of Vascular Anticoagulant-Alpha (Vac-Alpha) to Planar Phospholipid-Bilayers.* Journal of Biological Chemistry, 1990. **265**(9): p. 4923-4928.
36. Billy, D., et al., *Anticoagulant membrane-degrading effects of secretory (non-pancreatic) phospholipase A2 are inhibited in plasma.* Thrombosis and Haemostasis, 2002. **87**(6): p. 978-984.

37. Richter, R.P., et al., *On the kinetics of adsorption and two-dimensional self-assembly of annexin A5 on supported lipid bilayers.* Biophysical Journal, 2005. **89**(5): p. 3372-3385.
38. Reimhult, E., F. Hook, and B. Kasemo, *Intact vesicle adsorption and supported biomembrane formation from vesicles in solution: Influence of surface chemistry, vesicle size, temperature, and osmotic pressure.* Langmuir, 2003. **19**(5): p. 1681-1691.
39. Johnson, J.M., et al., *Early steps of supported bilayer formation probed by single vesicle fluorescence assays.* Biophysical Journal, 2002. **83**(6): p. 3371-3379.
40. Cremer, P.S., Boxer S. , *Formation and Spreading of Lipid Bilayers on Glass Surfaces* J. Phys. Chem. B., 1999. **103**: p. 2554-2559.
41. Cuypers, P.A., Janssen, M.P., Kop, J.M.M., Hermens W.Th., Hemker H.C.,, *Temperature Dependent Transitions in Several Phospholipids Measured by Ellipsometry.* Surface Science, 1980. **96**: p. 555-563.
42. Cuypers, P.A., et al., *The Adsorption-Kinetics of Proteins at Liquid-Solid Interfaces Measured by Ellipsometry.* Abstracts of Papers of the American Chemical Society, 1986. **192**: p. 32-Coll.
43. Benes, M., et al., *Surface-dependent transitions during self-assembly of phospholipid membranes on mica, silica, and glass.* Langmuir, 2004. **20**(23): p. 10129-10137.
44. Richter, R.P. and A.R. Brisson, *Following the formation of supported lipid bilayers on mica: A study combining AFM, QCM-D, and ellipsometry.* Biophysical Journal, 2005. **88**(5): p. 3422-3433.
45. Rowe, E.S., *Lipid chain length and temperature dependence of ethanol-phosphatidylcholine interactions.* Biochemistry, 2002. **22**(14): p. 3299-3305.
46. Simon, S.A., and and T. J. McIntosh, *Interdigitated hydrocarbon chain packing causes the biphasic transition behavior in lipid/alcohol suspensions* Biochimica et Biophysica Acta (BBA) - Biomembranes, 1984. **773**: p. 169-172.
47. Baber, J., J.F. Ellena, and D.S. Cafiso, *Distribution of General Anesthetics in Phospholipid Bilayers Determined Using 2H NMR and 1H-1H NOE Spectroscopy.* Biochemistry, 2002. **34**(19): p. 6533-6539.
48. Giesen, P.L.A., et al., *Membrane-Mediated Assembly of the Prothrombinase Complex.* Journal of Biological Chemistry, 1991. **266**(28): p. 18720-18725.
49. Mou, J., et al., *Alcohol Induces Interdigitated Domains in Unilamellar Phosphatidylcholine Bilayers.* Biochemistry, 2002. **33**(33): p. 9981-9985.
50. Miszta, A., et al., *Combination of ellipsometry, laser scanning microscopy and Z-scan fluorescence correlation spectroscopy elucidating interaction of cryptdin-4 with supported phospholipid bilayers.* Journal of Peptide Science, 2007.
51. Przybylo, M., et al., *Lipid diffusion in giant unilamellar vesicles is more than 2 times faster than in supported phospholipid bilayers under identical conditions.* Langmuir, 2006. **22**(22): p. 9096-9099.
52. Dertinger, T., et al., *Surface sticking and lateral diffusion of lipids in supported bilayers.* Langmuir, 2006. **22**(22): p. 9339-9344.
53. Mou, J.X., et al., *Alcohol Induces Interdigitated Domains in Unilamellar Phosphatidylcholine Bilayers.* Biochemistry, 1994. **33**(33): p. 9981-9985.
54. Zoya, V.L. and T.C. David, *Revisiting lipid - general anesthetic interactions (I): Thinned domain formation in supported planar bilayers induced by halothane and ethanol.* Canadian Journal of Chemistry, 2004. **82**: p. 1128-1138.
55. Miszta, A., et al., *Absence of Ethanol-Induced Interdigitation in Supported Phospholipid Bilayers on Silica Surfaces.* Langmuir, 2008. **24**(1): p. 19-21.

56. Benes, M., et al., *Muscovite (mica) allows the characterisation of supported Bilayers by ellipsometry and confocal fluorescence correlation spectroscopy.* Biological Chemistry, 2002. **383**(2): p. 337-341.
57. Enderlein, J., et al., *Performance of fluorescence correlation spectroscopy for measuring diffusion and concentration.* Chemphyschem, 2005. **6**(11): p. 2324-2336.
58. Enderlein, J., et al., *Art and artefacts of fluorescence correlation spectroscopy.* Current Pharmaceutical Biotechnology, 2004. **5**(2): p. 155-161.
59. Enderlein, J., et al., *Statistical analysis of diffusion coefficient determination by fluorescence correlation spectroscopy.* Journal of Fluorescence, 2005. **15**(3): p. 415-422.
60. Benda, A., et al., *Fluorescence lifetime correlation spectroscopy combined with lifetime tuning: New perspectives in supported phospholipid bilayer research.* Langmuir, 2006. **22**(23): p. 9580-9585.
61. Enderlein, J., *Autowave Propagation in a Piecewise Linearized Schlogl Model with Inhomogeneously Distributed Catalyst.* Physics Letters A, 1991. **156**(7-8): p. 429-435.
62. Enderlein, J., *Theoretical study of detection of a dipole emitter through an objective with high numerical aperture.* Optics Letters, 2000. **25**(9): p. 634-636.
63. Enderlein, J. and W.P. Ambrose, *Optical collection efficiency function in single-molecule detection experiments.* Applied Optics, 1997. **36**(22): p. 5298-5302.
64. Gregor, I., D. Patra, and J. Enderlein, *Optical saturation in fluorescence correlation spectroscopy under continuous-wave and pulsed excitation.* Chemphyschem, 2005. **6**(1): p. 164-170.
65. Dertinger, T., et al., *Two-focus fluorescence correlation spectroscopy: A new tool for accurate and absolute diffusion measurements.* Chemphyschem, 2007. **8**(3): p. 433-443.
66. Benda, A., et al., *How to determine diffusion coefficients in planar phospholipid systems by confocal fluorescence correlation spectroscopy.* Langmuir, 2003. **19**(10): p. 4120-4126.
67. Schwille, P., et al., *Molecular dynamics in living cells observed by fluorescence correlation spectroscopy with one- and two-photon excitation.* Biophysical Journal, 1999. **77**(4): p. 2251-2265.
68. Korlach, J., et al., *Characterization of lipid bilayer phases by confocal microscopy and fluorescence correlation spectroscopy.* Proceedings of the National Academy of Sciences of the United States of America, 1999. **96**(15): p. 8461-8466.
69. Humpolickova, J., et al., *Probing diffusion laws within cellular membranes by Z-scan fluorescence correlation spectroscopy.* Biophysical Journal, 2006. **91**(3): p. L23-L25.
70. Widengren, J. and R. Rigler, *Review - Fluorescence correlation spectroscopy as a tool to investigate chemical reactions in solutions and on cell surfaces.* Cellular and Molecular Biology, 1998. **44**(5): p. 857-879.
71. Widengren, J. and P. Thyberg, *FCS cell surface measurements - Photophysical limitations and consequences on molecular ensembles with heterogenic mobilities.* Cytometry Part A, 2005. **68A**(2): p. 101-112.
72. Kahya, N., et al., *Lipid domain formation and dynamics in giant unilamellar vesicles explored by fluorescence correlation spectroscopy.* Journal of Structural Biology, 2004. **147**(1): p. 77-89.

73. Bacia, K., et al., *Studying SNARE proteins incorporated into giant unilamellar vesicles by confocal imaging and fluorescence (cross-)correlation spectroscopy.* Biophysical Journal, 2004. **86**(1): p. 196A-196A.
74. Bacia, K., et al., *SNAREs prefer liquid-disordered over "raft" (liquid-ordered) domains when reconstituted into giant unilamellar vesicles.* Journal of Biological Chemistry, 2004. **279**(36): p. 37951-37955.
75. Bacia, K., P. Schwille, and T. Kurzchalia, *Sterol structure determines the separation of phases and the curvature of the liquid-ordered phase in model membranes.* Proceedings of the National Academy of Sciences of the United States of America, 2005. **102**(9): p. 3272-3277.
76. Kahya, N., et al., *Reconstitution of membrane proteins into giant unilamellar vesicles via peptide-induced fusion.* Biophysical Journal, 2001. **81**(3): p. 1464-1474.
77. Horton, M.R., J. Radler, and A.P. Gast, *Phase behavior and the partitioning of caveolin-1 scaffolding domain peptides in model lipid bilayers.* Journal of Colloid and Interface Science, 2006. **304**(1): p. 67-76.
78. Chiantia, S., et al., *Effects of ceramide on liquid-ordered domains investigated by simultaneous AFM and FCS.* Biophysical Journal, 2006. **90**(12): p. 4500-4508.
79. Chiantia, S., et al., *Combined AFM and two-focus SFCS study of raft-exhibiting model membranes.* Chemphyschem, 2006. **7**(11): p. 2409-2418.
80. Elson, E. and D. Magde, *Fluorescence Correlation Spectroscopy. I.Conceptual Basis and Theory.* Biopolymers, 1974. **13**: p. 1-27.
81. Magde, D. and E. Elson, *Fluorescence Correlation Spectroscopy. II.An Experimental Realization.* Biopolymers, 1974. **13**: p. 29-61.
82. Magde, D., E. Elson, and W.W. Webb, *Thermodynamic fluctuations in a reacting system - measurement by fluorescence correlation spectroscopy.* Physical Review Letters, 1972. **29**(11): p. 705-708.
83. Ehrenber.M and R. Rigler, *ROTATIONAL BROWNIAN-MOTION AND FLUORESCENCE INTENSITY FLUCTUATIONS.* Chemical Physics, 1974. **4**(3): p. 390-401.
84. Thompson, N.L., *Fluorescence Correlation Spectroscopy*, in *Topics in Fluorescence Spectroscopy*, J.R. Lakowicz, Editor. 1991, Plenum Press: New York. p. 337-378.
85. Schwille, P., F. Oehlenschlager, and N.G. Walter, *Quantitative hybridization kinetics of DNA probes to RNA in solution followed by diffusional fluorescence correlation analysis.* Biochemistry, 1996. **35**(31): p. 10182-10193.
86. Wohland, T., R. Rigler, and H. Vogel, *The standard deviation in fluorescence correlation spectroscopy.* Biophysical Journal, 2001. **80**(6): p. 2987-2999.
87. Enderlein, J., *Dependence of the optical saturation of fluorescence on rotational diffusion.* Chemical Physics Letters, 2005. **410**(4-6): p. 452-456.
88. Enderlein, J., *Path integral approach to fluorescence correlation experiments.* Physics Letters A, 1996. **221**(6): p. 427-433.
89. Ries, J. and P. Schwille, *Studying slow membrane dynamics with continuous wave scanning fluorescence correlation spectroscopy.* Biophysical Journal, 2006. **91**(5): p. 1915-1924.
90. Palmer, A.G. and N.L. Thompson, *Optical Spatial Intensity Profiles for High-Order Auto- Correlation in Fluorescence Spectroscopy.* Applied Optics, 1989. **28**(6): p. 1214-1220.

91. Sorscher, S.M. and M.P. Klein, *Profile of a Focused Collimated Laser-Beam near the Focal Minimum Characterized by Fluorescence Correlation Spectroscopy.* Review of Scientific Instruments, 1980. **51**(1): p. 98-102.
92. Domanov, Y.A. and P.K.J. Kinnunen, *Antimicrobial peptides temporins B and L induce formation of tubular lipid protrusions from supported phospholipid bilayers.* Biophysical Journal, 2006. **91**(12): p. 4427-4439.
93. Sood, R., Y. Domanov, and P.K.J. Kinnunen, *Fluorescent temporin B derivative and its binding to liposomes.* Journal of Fluorescence, 2007. **17**(2): p. 223-234.
94. Zhao, H.X., et al., *Binding of endostatin to phosphatidylserine-containing membranes and formation of amyloid-like fibers.* Biochemistry, 2005. **44**(8): p. 2857-2863.
95. Burns, A.R., D.J. Frankel, and T. Buranda, *Local mobility in lipid domains of supported bilayers characterized by atomic force microscopy and fluorescence correlation spectroscopy.* Biophysical Journal, 2005. **89**(2): p. 1081-1093.
96. Forstner, M.B., et al., *Lipid lateral mobility and membrane phase structure modulation by protein binding.* Journal of the American Chemical Society, 2006. **128**(47): p. 15221-15227.
97. Balgavy, P., et al., *X-ray diffraction and neutron scattering studies of amphiphile - Lipid bilayer organization.* Cellular & Molecular Biology Letters, 2001. **6**(2A): p. 283-290.
98. Deniaud, A., et al., *Voltage-dependent anion channel transports calcium ions through biomimetic membranes.* Langmuir, 2007. **23**(7): p. 3898-3905.
99. Vacklin, H.P., et al., *Composition of supported model membranes determined by neutron reflection.* Langmuir, 2005. **21**(7): p. 2827-2837.
100. Zhao, H., et al., *Interaction of the antimicrobial peptide pheromone Plantaricin A with model membranes: Implications for a novel mechanism of action.* Biochimica Et Biophysica Acta-Biomembranes, 2006. **1758**(9): p. 1461-1474.
101. Mally, M., et al., *The response of giant phospholipid vesicles to pore-forming peptide melittin.* Biochimica Et Biophysica Acta-Biomembranes, 2007. **1768**(5): p. 1179-1189.
102. Bradrick, T.D., A. Philippetis, and S. Georghiou, *Stopped-flow fluorometric study of the interaction of melittin with phospholipid bilayers: Importance of the physical state of the bilayer and the acyl chain length.* Biophysical Journal, 1995. **69**(5): p. 1999-2010.
103. Zasloff, M., *Antimicrobial peptides of multicellular organisms.* Nature, 2002. **415**(6870): p. 389-395.
104. Blondelle, S.E., K. Lohner, and M.-I. Aguilar, *Lipid-induced conformation and lipid-binding properties of cytolytic and antimicrobial peptides: determination and biological specificity.* Biochimica et Biophysica Acta (BBA) - Biomembranes, 1999. **1462**(1-2): p. 89-108.
105. Hancock, R.E.W., and Scott, M.G., , *The role of antimicrobial peptides in animal defenses.* PNAS, 2000. **97**: p. 8856-8861.
106. Bowdish, D.M.E., et al., *Immunomodulatory activities of small host defense peptides.* Antimicrobial Agents and Chemotherapy, 2005. **49**(5): p. 1727-1732.
107. Hancock, R.E.W. and G. Diamond, *The role of cationic antimicrobial peptides in innate host defences.* Trends in Microbiology, 2000. **8**(9): p. 402-410.
108. Brown, K.L. and R.E.W. Hancock, *Cationic host defense (antimicrobial) peptides.* Current Opinion in Immunology, 2006. **18**(1): p. 24-30.

109. Bowdish, D.M.E., D.J. Davidson, and R.E.W. Hancock, *A re-evaluation of the role of host defence peptides in mammalian immunity.* Current Protein & Peptide Science, 2005. **6**(1): p. 35-51.
110. Bechinger, B., *The structure, dynamics and orientation of antimicrobial peptides in membranes by multidimensional solid-state NMR spectroscopy.* Biochimica et Biophysica Acta, 1999. **1462**: p. 157-183.
111. Shai, Y., *Mechanism of the binding, insertion and destabilization of phospholipid bilayer membranes by alfa-helical antimicrobial and cell non-selective membrane-lytic peptides.* Biochimica Et Biophysica Acta, 1999. **1462**: p. 55-70.
112. Ramamoorthy, A., et al., *Solid-state NMR investigation of the membrane-disrupting mechanism of antimicrobial peptides MSI-78 and MSI-594 derived from magainin 2 and melittin.* Biophysical Journal, 2006. **91**(1): p. 206-216.
113. Blondelle, S.E., et al., *Influence of cell membrane lipid composition on the specificity of antimicrobial peptides.* Biophysical Journal, 1999. **76**(1): p. A68-A68.
114. Hancock, R.E.W. and D.S. Chapple, *Peptide antibiotics.* Antimicrobial Agents and Chemotherapy, 1999. **43**(6): p. 1317-1323.
115. Lehmann, J., et al., *Antitumor activity of the antimicrobial peptide Magainin II against bladder cancer cell lines.* European Urology, 2006. **50**(1): p. 141-147.
116. Cruciani, R.A., et al., *Antibiotic Magainins Exert Cytolytic Activity against Transformed-Cell Lines through Channel Formation.* Proceedings of the National Academy of Sciences of the United States of America, 1991. **88**(9): p. 3792-3796.
117. Dathe, M. and T. Wieprecht, *Structural features of helical antimicrobial peptides: their potential to modulate activity on model membranes and biological cells.* Biochimica et Biophysica Acta (BBA) - Biomembranes, 1999. **1462**(1-2): p. 71-87.
118. Limjaroen, P., et al., *Development of a food packaging coating material with antimicrobial properties.* Journal of Plastic Film & Sheeting, 2003. **19**(2): p. 95-109.
119. Rydlo, T., J. Miltz, and A. Mor, *Eukaryotic antimicrobial peptides: Promises and premises in food safety.* Journal of Food Science, 2006. **71**(9): p. R125-R135.
120. Torrens, F., et al., *Negatively cooperative binding of melittin to neutral phospholipid vesicles.* Journal of Molecular Structure, 2007. **834**: p. 216-228.
121. Beschiaschvili, G. and J. Seelig, *Melittin Binding to Mixed Phosphatidylglycerol Phosphatidylcholine Membranes.* Biochemistry, 1990. **29**(1): p. 52-58.
122. Popplewell, J.F., et al., *Quantifying the effects of melittin on liposomes.* Biochimica Et Biophysica Acta-Biomembranes, 2007. **1768**(1): p. 13-20.
123. Figueredo, S.M., et al., *Anionic Amino Acids near the Pro-{alpha}-defensin N Terminus Mediate Inhibition of Bactericidal Activity in Mouse Pro-cryptdin-4.* J. Biol. Chem., 2009. **284**(11): p. 6826-6831.
124. Klocek, G., et al., *Thermodynamics of Melittin Binding to Lipid Bilayers. Aggregation and Pore Formation&#x2020.* Biochemistry, 2009. **48**(12): p. 2586-2596.
125. Shaw, J.E., et al., *Cationic peptide-induced remodelling of model membranes: Direct visualization by in situ atomic force microscopy.* Journal of Structural Biology, 2008. **162**(1): p. 121-138.
126. Raghuraman, H. and A. Chattopadhyay, *Melittin: A membrane-active peptide with diverse functions.* Bioscience Reports, 2007. **27**(4-5): p. 189-223.
127. Terwilliger, T.C. and D. Eisenberg, *The structure of melittin. I. Structure determination and partial refinement.* J. Biol. Chem., 1982. **257**(11): p. 6010-6015.

128. Terwilliger, T.C., L. Weissman, and D. Eisenberg, *The structure of melittin in the form I crystals and its implication for melittin's lytic and surface activities.* 1982. **37**(1): p. 353-361.
129. Matsuzaki, K., et al., *Interactions of an antimicrobial peptide, magainin 2, with outer and inner membranes of Gram-negative bacteria.* Biochimica Et Biophysica Acta-Biomembranes, 1997. **1327**(1): p. 119-130.
130. Papo, N. and Y. Shai, *Exploring Peptide Membrane Interaction Using Surface Plasmon Resonance: Differentiation between Pore Formation versus Membrane Disruption by Lytic Peptides&#x2020.* Biochemistry, 2003. **42**(2): p. 458-466.
131. Tanya, S., et al., *Bilayer localization of membrane-active peptides studied in biomimetic vesicles by visible and fluorescence spectroscopies.* European Journal of Biochemistry, 2003. **270**(22): p. 4478-4487.
132. Brogden, K.A., *Antimicrobial peptides: Pore formers or metabolic inhibitors in bacteria?* Nature Reviews Microbiology, 2005. **3**(3): p. 238-250.
133. Sheynis, T., et al., *Bilayer localization of membrane-active peptides studied in biomimetic vesicles by visible and fluorescence spectroscopies.* European Journal of Biochemistry, 2003. **270**(22): p. 4478-4487.
134. Ouellette, A.J. and M.E. Selsted, *Paneth cell defensins: endogenous peptide components of intestinal host defense.* FASEB J., 1996. **10**(11): p. 1280-1289.
135. Satchell, D.P., et al., *Interactions of Mouse Paneth Cell alpha -Defensins and alpha -Defensin Precursors with Membranes. PROSEGMENT INHIBITION OF PEPTIDE ASSOCIATION WITH BIOMIMETIC MEMBRANES.* J. Biol. Chem., 2003. **278**(16): p. 13838-13846.
136. Tanabe, H., et al., *Structure-Activity Determinants in Paneth Cell {alpha}-Defensins: LOSS-OF-FUNCTION IN MOUSE CRYPTDIN-4 BY CHARGE-REVERSAL AT ARGININE RESIDUE POSITIONS.* J. Biol. Chem., 2004. **279**(12): p. 11976-11983.
137. Hadjicharalambous, C., et al., *Mechanisms of α-Defensin Bactericidal Action: Comparative Membrane Disruption by Cryptdin-4 and Its Disulfide-Null Analogue&#x2020.* Biochemistry, 2008. **47**(47): p. 12626-12634.
138. Rosengren, K.J., et al., *Structural and Functional Characterization of the Conserved Salt Bridge in Mammalian Paneth Cell {alpha}-Defensins: SOLUTION STRUCTURES OF MOUSE CRYPTDIN-4 AND (E15D)-CRYPTDIN-4.* J. Biol. Chem., 2006. **281**(38): p. 28068-28078.
139. Tamba, Y. and M. Yamazaki, *Single Giant Unilamellar Vesicle Method Reveals Effect of Antimicrobial Peptide Magainin 2 on Membrane Permeability&#x2020.* Biochemistry, 2005. **44**(48): p. 15823-15833.
140. Weeks, C.S., et al., *Matrix Metalloproteinase-7 Activation of Mouse Paneth Cell Pro-{alpha}-defensins: SER43{downarrow}ILE44 PROTEOLYSIS ENABLES MEMBRANE-DISRUPTIVE ACTIVITY.* J. Biol. Chem., 2006. **281**(39): p. 28932-28942.
141. Satchell, D.P., et al., *Quantitative interactions between cryptdin-4 amino terminal variants and membranes.* Peptides, 2003. **24**(11): p. 1795-1805.
142. Wawrezinieck, L., et al., *Fluorescence correlation spectroscopy diffusion laws to probe the submicron cell membrane organization.* Biophysical Journal, 2005. **89**(6): p. 4029-4042.
143. Ladokhin, A.S. and S.H. White, *'Detergent-like' permeabilization of anionic lipid vesicles by melittin.* Biochimica Et Biophysica Acta-Biomembranes, 2001. **1514**(2): p. 253-260.

144. Yang, L., et al., *Barrel-stave model or toroidal model? A case study on melittin pores.* Biophysical Journal, 2001. **81**(3): p. 1475-1485.
145. Rex, S., *Pore formation induced by the peptide melittin in different lipid vesicle membranes.* Biophysical Chemistry, 1996. **58**(1-2): p. 75-85.
146. Machan, R., Miszta A., Hermens W. Th., Hof M.,, *Real-time monitoring of melittin induced pore and tubule formation from supported lipid bilayers and its physiological relevance.* Biochimica et Biophysica Acta - Biomembranes 2009. submitted.
147. Grandbois, M., H. Clausen-Schaumann, and H. Gaub, *Atomic force microscope imaging of phospholipid bilayer degradation by phospholipase A(2).* Biophysical Journal, 1998. **74**(5): p. 2398-2404.
148. Bayerl, T.M., et al., *Specular Reflection of Neutrons at Phospholipid Monolayers - Changes of Monolayer Structure and Headgroup Hydration at the Transition from the Expanded to the Condensed Phase State.* Biophysical Journal, 1990. **57**(5): p. 1095-1098.
149. Johnson, S.J., et al., *Structure of an Adsorbed Dimyristoylphosphatidylcholine Bilayer Measured with Specular Reflection of Neutrons.* Biophysical Journal, 1991. **59**(2): p. 289-294.
150. Almeida, P.F., Vaz, W.L., Thompson T.E.,, *Lateral diffusion and percolation in two-phase, two-component lipid bilayers. Topology of the solid-phase domains in-plane and across the lipid bilayer.* Biochemistry, 1992. **31**: p. 7198-210.